CHAPTER 2 THEORIES AND LITERATURE REVIEWS

This chapter covers three large subjects, multiphase steels, yield functions and hardening models, formability characterization and modeling of failure. Overview and introduction for multiphase steels, the classification of microstructure and mechanical properties are firstly given. The specific fracture behavior of these steels and the phase transformation induced plasticity of TRIP steel are also discussed. The next session concerns different important formability characterization methods. These sheet metal forming tests were used to verify the numerical simulations. The failure criteria and damage models treated in this work are outlined in the last session.

2.1 Multiphase Steels

Two major factors have been driving the development of new steel products for the automotive industry. The first is the desire for thickness reduction of steel sheet due to fuel economy. To attain this aspect, steel products with higher strength and formability are needed. The second is the safety performance with regard to increased ability for energy absorption. For these aspects, Advanced High Strength Steel (AHSS) with increased uniform and total elongation are the first choice for development activities. Multiphase steels as dual phase steel, TRIP steel, complex steel and martensitic steel are in the class of the AHSS grade. The multiphase steels are superior in strength and ductility combination as compared with conventional High Strength Steel (HSS) and High Strength Low Alloy Steel (HSLA). The minimum tensile strengths range from 500 to 800 MPa. These steels are easier to form than HSLA grades with similar initial yield strengths but they have much higher final part strength. Conventional HSSs are hardened by solid solution, precipitation or grain refinement, while multiphase steels are strengthened by phase transformation, and the microstructure that may include martensite, bainite and retained austenite. Figure 2.1 shows typical mechanical properties ranges of different steel grades. It is obvious that AHSSs offer higher strength values than HSSs. The strength-ductility relationship of AHSS is also improved. For the new developed high Mn steels an extraordinary strength-ductility relationship with a product Rm x A80 up to 50000 MPa*% is expected. [1]

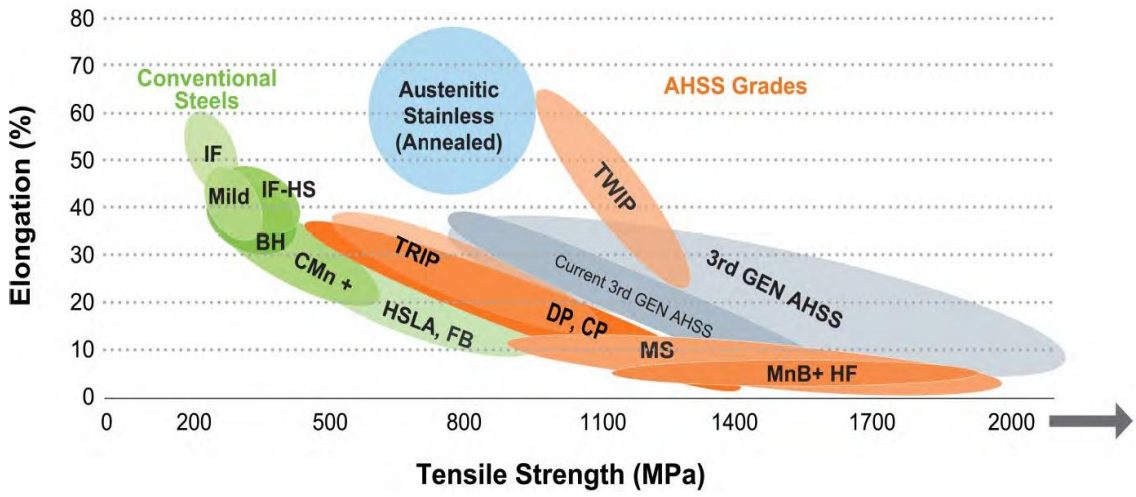

Figure 2.1 Tensile strength and total elongation of different steel grades in comparison [2]

AHS steels are complex, sophisticated materials, with carefully selected chemical compositions and multiphase microstructures resulting from precisely controlled heating and cooling processes. Various strengthening mechanisms are employed to achieve a range of strength, ductility, toughness, and fatigue properties.

The AHS steel family includes Dual Phase (DP), Complex-Phase (CP), Ferritic-Bainitic (FB), Martensitic (MS or MART), Transformation-Induced Plasticity (TRIP), Hot-Formed (HF), and Twinning-Induced Plasticity (TWIP). These 1st and 2nd Generation AHSS grades are uniquely qualified to meet the functional performance demands of certain parts. For example, DP and TRIP steels are excellent in the crash zones of the car for their high energy absorption. For structural elements of the passenger compartment, extremely high-strength steels, such as Martensitic and boron-based Press Hardened Steels (PHS) result in improved safety performance. Recently there has been increased funding and research for the development of the "3rd Generation" of AHSS. These are steels with improved strength-ductility combinations compared to present grades, with potential for more efficient joining capabilities, at lower costs. These grades will reflect unique alloys and microstructures to achieve the desired properties. The broad range of properties is best illustrated by the famous Global Formability Diagram, captured in Figure 2.1. [2]

Steels with yield strength levels in excess of 550 MPa are generally referred to as AHS steel. These steels are also sometimes called "ultrahigh-strength steels" for tensile strengths exceeding 780 MPa. AHS steel with tensile strength of at least 1000 MPa are often called "GigaPascal steel" (1000 MPa = 1GPa). Please note another category of steels, represented with a bubble in Figure 2.1, Austenitic Stainless Steel. These materials have excellent strength combined with excellent ductility, and thus meet many vehicle functional requirements. Due to alloying content, however, they are expensive choices for many components, and joining can be a challenge. Third Generation AHSS seeks to offer comparable or improved capabilities at significantly lower cost. [2]

2.1.1 Metallurgy of AHS steel [2]

Manufacturers and users of steel products generally understand the fundamental metallurgy of conventional low- and high-strength steels. Section 2.B. provides a brief description of these common steel types. Since the metallurgy and processing of AHSS grades are somewhat novel compared to conventional steels, they are described here to provide a baseline understanding of how their remarkable mechanical properties evolve from their unique processing and structure. All AHSS are produced by controlling the chemistry and cooling rate from the austenite or austenite plus ferrite phase, either on the runout table of the hot mill (for hot-rolled products) or in the cooling section of the continuous annealing furnace (continuously annealed or hot-dip coated products). Research has provided chemical and processing combinations that have created many additional grades and improved properties within each type of AHSS.

2.1.1.1 Dual Phase (DP) Steel [2]

DP steels consist of a ferritic matrix containing a hard martensitic second phase in the form of islands. Increasing the volume fraction of hard second phases generally increases the strength. DP (ferrite plus martensite) steels are produced by controlled cooling from the austenite phase (in hot-rolled products) or from the two-phase ferrite plus austenite phase (for continuously annealed cold-rolled and hot-dip coated products) to transform some austenite to ferrite before a rapid cooling transforms the remaining

austenite to martensite. Due to the production process, small amount of other phases (Bainite and Retained Austenite) may be present. Depending on the composition and process route, steels requiring enhanced capability to resist cracking on a stretched edge (as typically measured by hole expansion capacity) can have a microstructure containing significant quantities of bainite. Figure 2.2 shows a schematic microstructure of DP steel, which contains ferrite plus islands of martensite. The soft ferrite phase is generally continuous, giving these steels excellent ductility. When these steels deform, strain is concentrated in the lower-strength ferrite phase surrounding the islands of martensite, creating the unique high initial work-hardening rate (n-value) exhibited by these steels. Figure 2.3 is an actual photo micrograph showing the ferrite and martensite constituents.

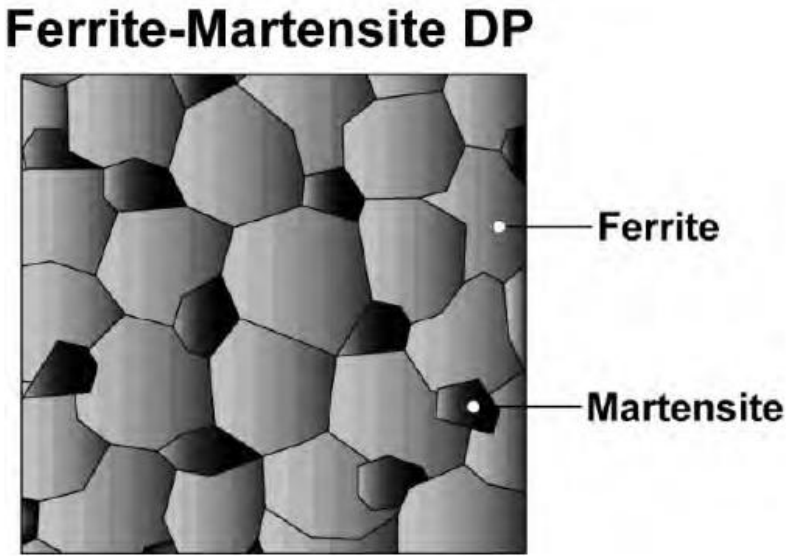

Figure 2.2 Schematic shows islands of martensite in a matrix of ferrite

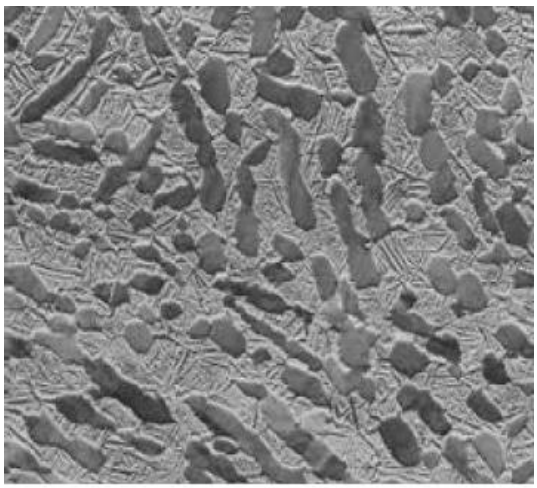

Figure 2.3 Photomicrograph of DP steel

The work hardening rate plus excellent elongation creates DP steels with much higher ultimate tensile strengths than conventional steels of similar yield strength. Figure 2.4 compares the engineering stress-strain curve for HSLA steel to a DP steel curve of similar yield strength. The DP steel exhibits higher initial work hardening rate, higher

ultimate tensile strength, and higher TS/YS ratio than a similar yield strength HSLA. Additional engineering and true stress-strain curves for DP steel grades are located in Figure 2.5.

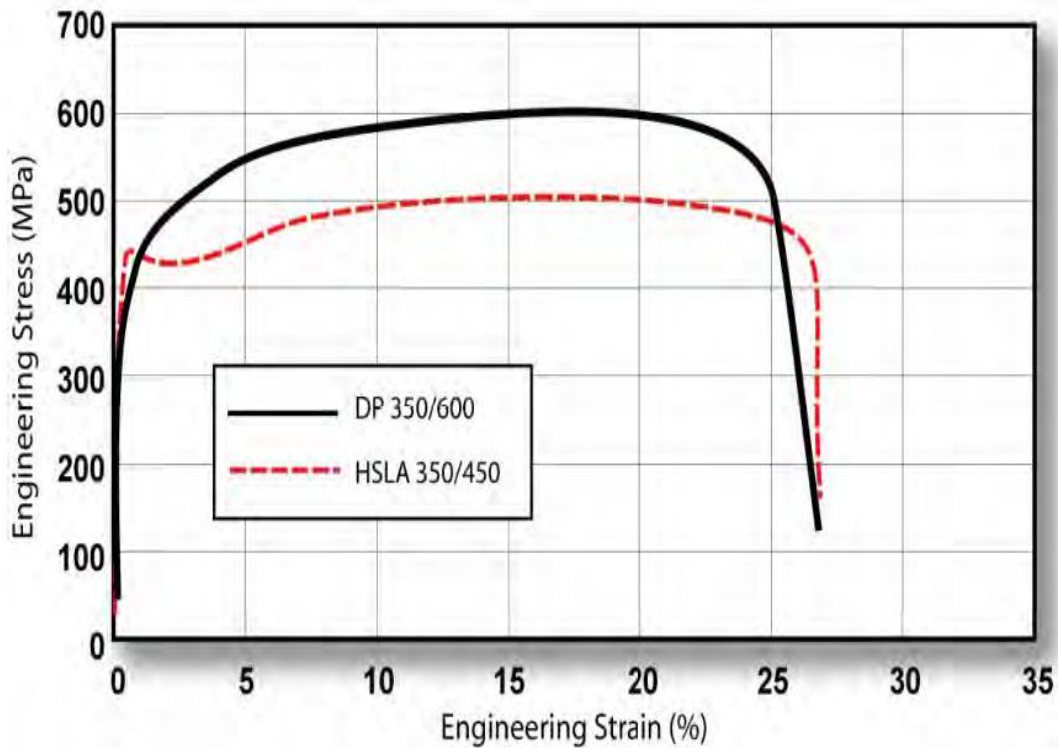

Figure 2.4 The DP 350/600 with higher TS than the HSLA 350/450K-1

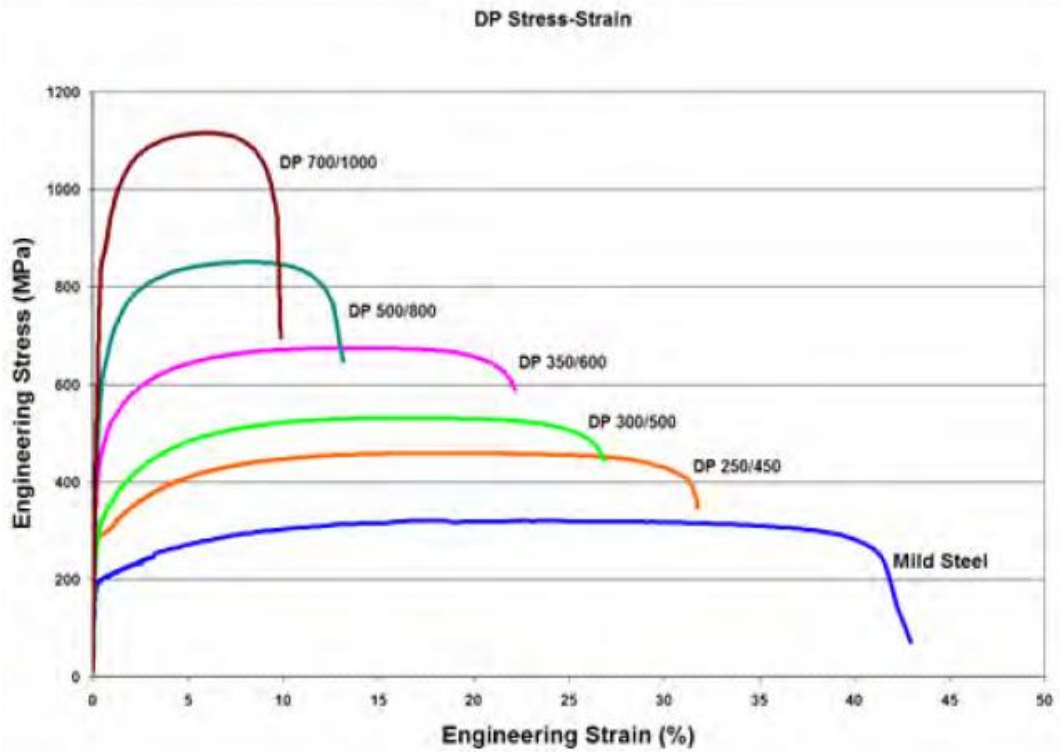

(a)

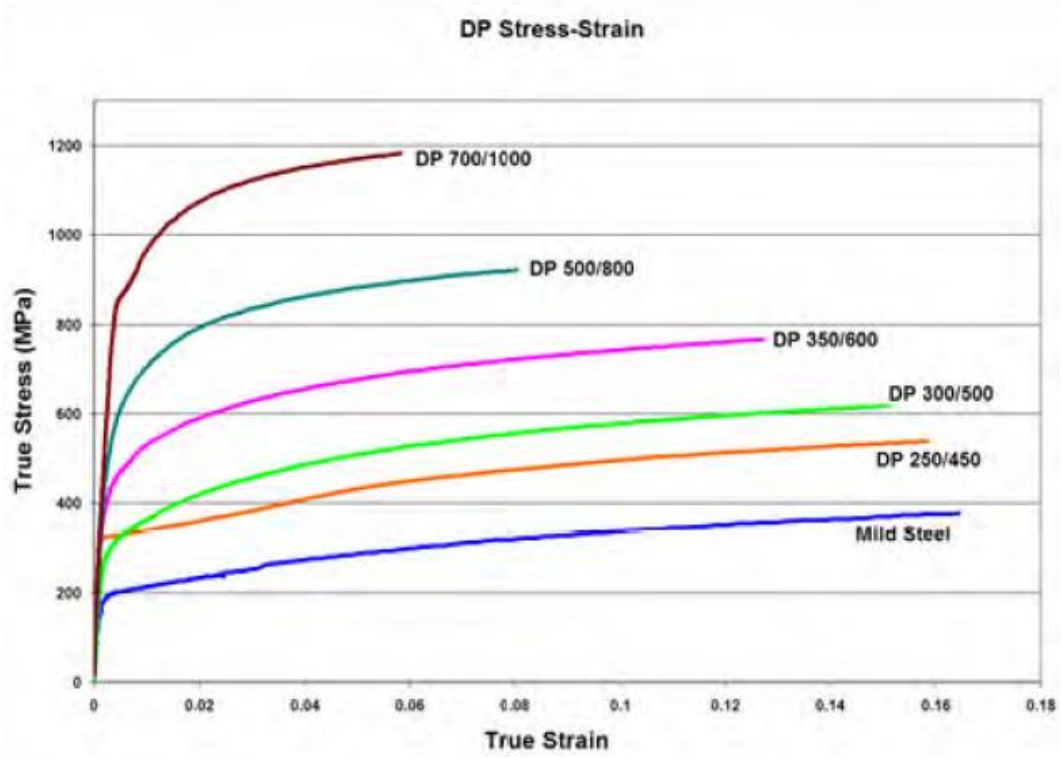

(b)

Figure 2.5 (a) Engineering stress-strain, (b) True stress-strain curves for DP steels

2.1.1.2 Transformation Induced Plasticity (TRIP) Steel [2]

The microstructure of TRIP steels is retained austenite embedded in a primary matrix of ferrite. In addition to a minimum of five volume percent of retained austenite, hard phases such as martensite and bainite are present in varying amounts. TRIP steels typically require the use of an isothermal hold at an intermediate temperature, which produces some bainite. The higher silicon and carbon content of TRIP steels also result in significant volume fractions of retained austenite in the final microstructure. Figure 2.6 shows a schematic of TRIP steel microstructure. Figure 2.7 is a micrograph of TRIP 690.

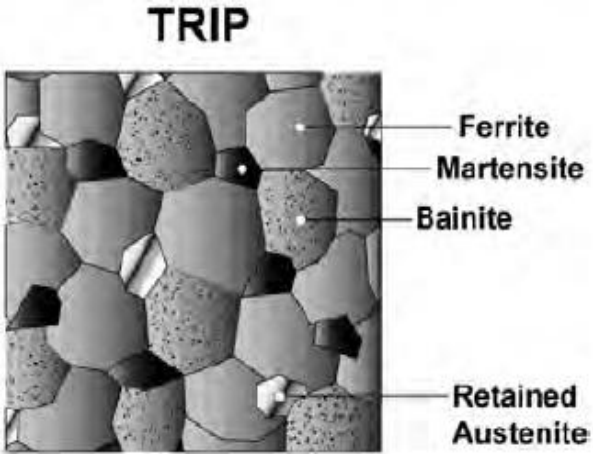

Figure 2.6 Bainite and retained austenite are additional phases in TRIP steels

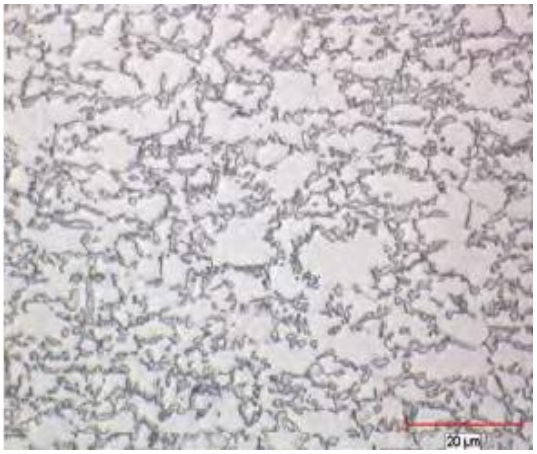

Figure 2.7 Micrograph of TRIP 690 steel

During deformation, the dispersion of hard second phases in soft ferrite creates a high work hardening rate, as observed in the DP steels. However, in TRIP steels the retained austenite also progressively transforms to martensite with increasing strain, thereby increasing the work hardening rate at higher strain levels. This is illustrated in Figure 2.8, where the engineering stress-strain behavior of HSLA, DP and TRIP steels of approximately similar yield strengths are compared. The TRIP steel has a lower initial work hardening rate than the DP steel, but the hardening rate persists at higher strains where work hardening of the DP begins to diminish. Additional engineering and true stress-strain curves for TRIP steel grades are located in Figure 2.9.

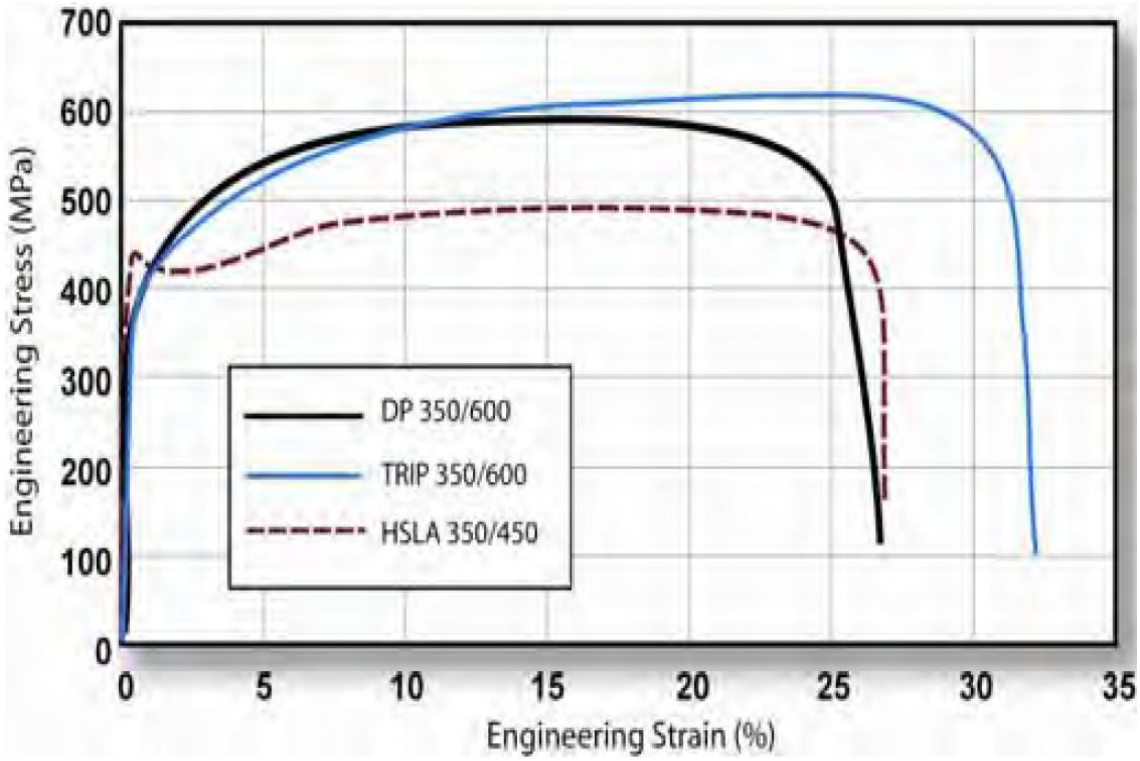

Figure 2.8 TRIP with a greater total elongation than DP and HSLA steel

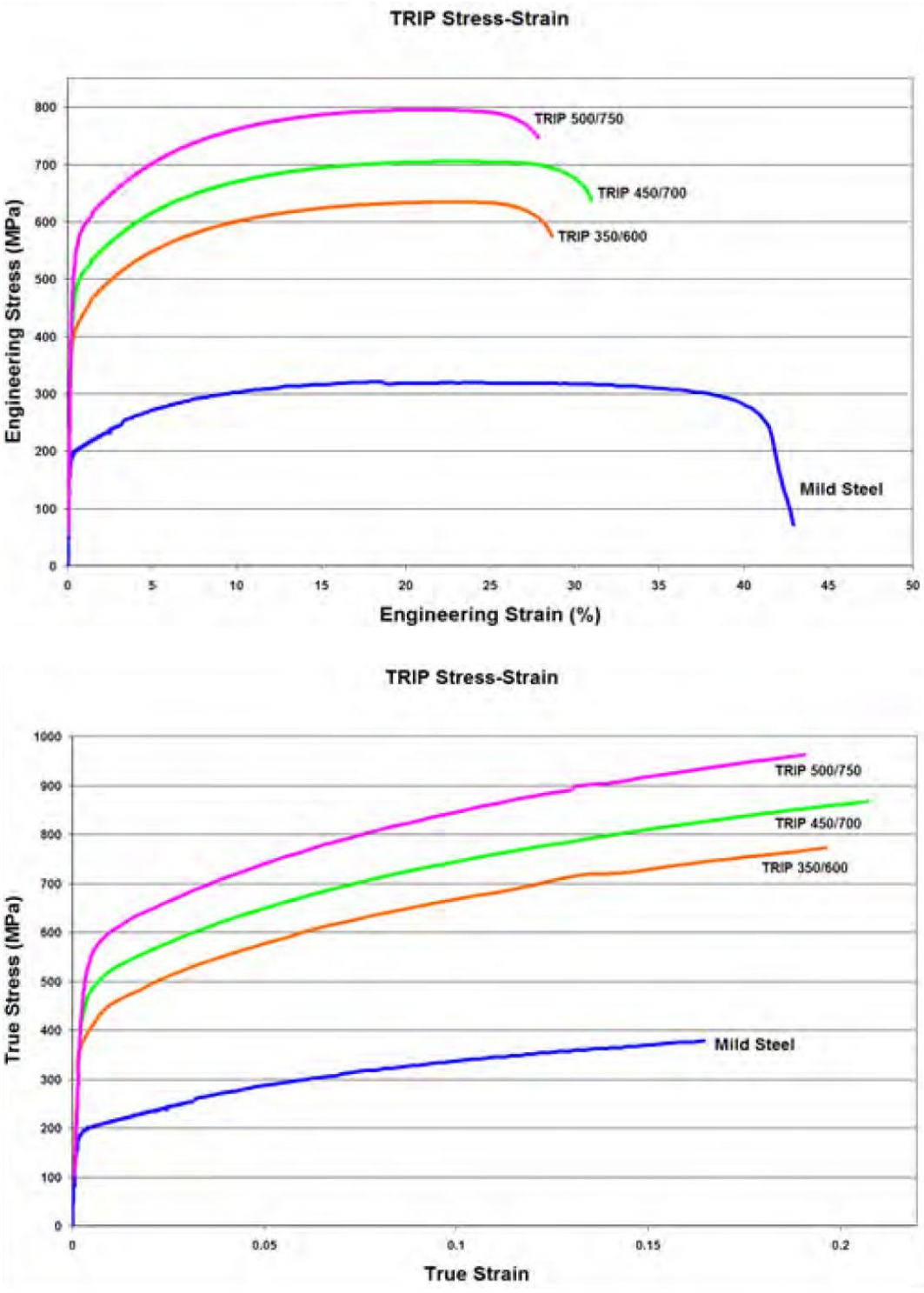

Figure 2.9 (a) Engineering stress-strain, (b) True stress-strain curves for TRIP steels

The work hardening rates of TRIP steels are substantially higher than for conventional HSS, providing significant stretch forming. This is particularly useful when designers take advantage of the high work hardening rate (and increased bake hardening effect) to design a part utilizing the as-formed mechanical properties. The high work hardening rate persists to higher strains in TRIP steels, providing a slight advantage over DP in the most severe stretch forming applications. TRIP steels use higher quantities of carbon than DP steels to obtain sufficient carbon content for stabilizing the retained austenite

phase to below ambient temperature. Higher contents of silicon and/or aluminium accelerate the ferrite/bainite formation. These elements assist in maintaining the necessary carbon content within the retained austenite. Suppressing the carbide precipitation during bainitic transformation appears to be crucial for TRIP steels. Silicon and aluminium are used to avoid carbide precipitation in the bainite region. The strain level at which retained austenite begins to transform to martensite is controlled by adjusting the carbon content. At lower carbon levels, the retained austenite begins to transform almost immediately upon deformation, increasing the work hardening rate and formability during the stamping process. At higher carbon contents, the retained austenite is more stable and begins to transform only at strain levels beyond those produced during forming.

2.1.2 Microstructure and Mechanical properties [1,2]

Figure 2.10 illustrates the microstructural characteristics during the strain hardening of different steels in comparison. Thus, DP steel has a high strain hardening directly after reaching the yield point. Because plastic flow begins simultaneously at many sites throughout the specimen, discontinuous yielding is suppressed. The work hardening process or the stress-strain relationship of DP steels associating with the deformation mechanisms can be separated into three stages. In the first stage, the work hardening rate is high because of the elimination of residual stresses in ferrite caused by the plastic incompressibility between two phases. The two constituent phases deform elastically. In the second stage, the work hardening rate of the ferrite is reduced as the plastic flow of the ferrite is constrained by the hard martensite particles. The ferritic phase deforms plastically, the harder martensitic phase continues to deform elastically. Finally, in the third stage, dislocation structures are formed and further deformation in the ferrite is governed by dynamic recovery and by eventual yielding of the martensite. Both phases deform now plastically

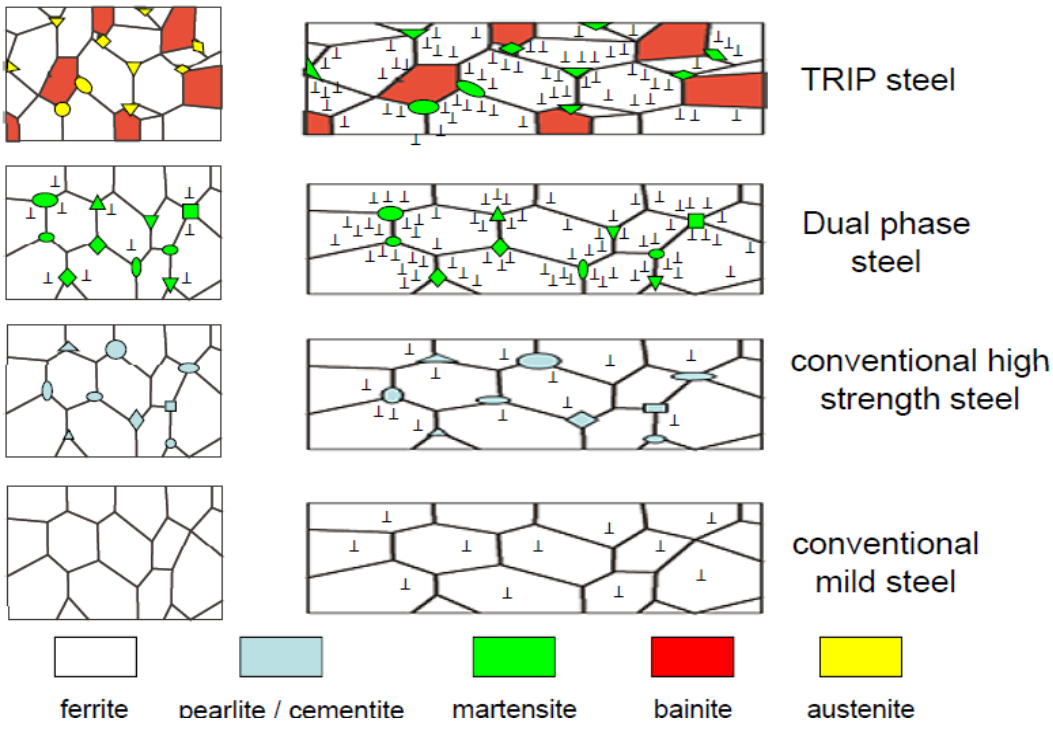

Figure 2.10 Schematic representation

2.2 Constitutive Models for Formability Behavior

In order to solve the complex boundary value problems and formability prediction for AHS steels, the finite element method (FEM) has been frequently used. FEM has especially played a significant role in optimizing process conditions in the forming industries. Application of the finite element method to sheet metal forming processes needs reliable constitutive models [3]. First, the initiation of plastic deformation of the sheet metal should be properly characterized by a yield criterion. The effect of yield criterion implemented into the finite element program is known to have a significant effect on the anisotropic nature of deformation, formability and so on. Second, plastic flow behavior after initiation of plastic deformation has to be described properly using the appropriate hardening law. The hardening law describes not only the simple isotropic evolution of the yield criterion, but also the transient behavior when the loading direction is changed. Finally, a failure criterion has to be identified to characterize the failure caused by the instability in sheet metal forming process. [4]

In the present study, finite element simulations will be carried out using various constitutive models to validate the formability of advanced high strength steels, characterize and validate the failure criterion. Simple tool geometry with less focus on process effects will be considered, but most of the work will be focused on the effect of the constitutive models on the deformation behavior. In terms of the yield criterion, which is one of the most important constitutive models in FEM analysis, three different yield criteria,namely, von Mises yield criterion [5], Hill's 1948 yield criterion [6] and Yld2000-2d [7] will be employed in order to predict the sheet metal formability of AHS steel. As for the hardening model, the swift hardening model [8], Voce [9] and modified Voce hardening model [10] will be used to characterize material flow behaviour. Both conventional uniaxial tensile tests and advanced balanced biaxial experiments using the hydraulic bulge test will be used to obtain the evolution of plastic deformation after initial yielding. The plane stress condition is frequently used to solve practical problems in sheet metal forming because it can reduce the complexity of the formulations. Therefore, in this study, the plane stress condition will be used for both the finite element model and the material model.

2.2.1 Yield Functions

A yield criterion is a postulated mathematical formula of the stress state which causes plastic deformation. Therefore, the general form of the criterion is expressed as a function of six independent stress components where

$$f\left(\sigma_{xx},\sigma_{yy},\sigma_{zz},\tau_{yz},\tau_{zx},\tau_{xy}\right)=\bar{\sigma} \tag{2.1}$$

Where $\bar{\sigma}$ is a equivalent stress determining the size of the yield criterion. The phenomenological yield models according to the von Mises [5], Hill'48 [6] and Yld2000-2d [7] yield criteria were considered in this work for describing plastic anisotropic behavior of both investigated AHS steels in this work. The anisotropy could have significant influences on local material properties and thus forming behavior of the steel. In order to model the material anisotropy in a sheet metal, variation of yield stress and *r*-values with respect to the rolling direction must be first studied. A brief overview of the applied yield models along with the methods for determining their corresponding parameters was discussed below.

2.2.1.1 Von Mises Yield Criterion

The fundamental quadratic isotropic yield criterion was introduced by von Mises in 1913 [5].The von Mises yield criterion is express with the second deviatoric invariant J_2,

$$J_2 = \frac{1}{2} S_{ij} S_{ij}$$

$$= \frac{1}{6}\left[\left(\sigma_{yy} - \sigma_{zz}\right)^2 + \left(\sigma_{zz} - \sigma_{xx}\right)^2 + \left(\sigma_{xx} - \sigma_{yy}\right)^2 \right] + \tau_{yz}^2 + \tau_{zx}^2 + \tau_{xy}^2$$

$$= \frac{1}{6}\left[\left(\sigma_1 - \sigma_2\right)^2 + \left(\sigma_2 - \sigma_3\right)^2 + \left(\sigma_3 - \sigma_1\right)^2 \right] \tag{2.2}$$

Where equations (2.1) and (2.2) denote the principle components. Then, the simple modelling of isotropic material was presented. Under general state of stress, the von Mises yield criterion can be expressed as

$$\left(\sigma_1 - \sigma_2\right)^2 + \left(\sigma_2 - \sigma_3\right)^2 + \left(\sigma_3 - \sigma_1\right)^2 = 2\bar{\sigma}^2 \tag{2.3}$$

or

$$\left(\sigma_{yy} - \sigma_{zz}\right)^2 + \left(\sigma_{zz} - \sigma_{xx}\right)^2 + \left(\sigma_{xx} - \sigma_{yy}\right)^2 + 6\left(\tau_{yz}^2 + \tau_{zx}^2 + \tau_{xy}^2\right) = 2\bar{\sigma}^2 \tag{2.4}$$

and under plane stress condition, the yield criterion can be further simplified to

$$\bar{\sigma}^2 = \sigma_{xx}^2 + \sigma_{xx}\sigma_{yy} + \sigma_{yy}^2 + 3\tau_{xy}^2 \tag{2.5}$$

where the stress component related with z-axis become all zero in equation 2.4, $\sigma_{zz} = \tau_{yz} = \tau_{zx} = 0$, $\bar{\sigma}$ is the effective stress and σ_{xx}, σ_{yy} and σ_{xy} are the in plane stresses. The effective stress, $\bar{\sigma}$ can be calculated from experimentally determined yield stress. Usually, a simple uniaxial tension test in the rolling direction was conducted.

2.2.1.2 Hill'48 Yield Criterion

The quadratic anisotropic yield criterion proposed by Hill [6] is one of the most widely used yield functions. The Hill'48 yield model assumes that a material exhibits three mutually orthogonal planes of symmetry. The principal axes of anisotropy are denoted as *x*, *y* and *z*, about which material properties have two-fold symmetry. This yield function has been successfully applied for modelling various kinds of steel sheets. The yield potential of the Hill'48 criterion can be represented by:

$$2f(\sigma) = F\left(\sigma_{yy} - \sigma_{zz}\right)^2 + G\left(\sigma_{zz} - \sigma_{xx}\right)^2 + H\left(\sigma_{xx} - \sigma_{yy}\right)^2 + 2(L\sigma_{yz}{}^2 + M\sigma_{zx}{}^2 + N\sigma_{xy}^2)$$

$$= 1 \tag{2.6}$$

Under plane stress condition $\left(\sigma_{zz} = \sigma_{yz} = \sigma_{zx} = 0\right)$, the Hill'48 model is simplified as:

$$2f(\sigma) = (G+H)\sigma_{xx}{}^2 + (F+H)\sigma_{yy}{}^2 - 2H\sigma_{xx}\sigma_{yy} + 2N\sigma_{xy}^2 = 1 \tag{2.7}$$

Where σ_{xx}, σ_{yy} and σ_{zz} are the stresses in the rolling (*x*), transverse (*y*) and thickness (*z*) directions respectively. σ_{xy}, σ_{yz} and σ_{zx} are the shear stresses in *xy*, *yz* and *zx* planes, respectively. *F*, *G*, *H* and *N* are the anisotropic coefficient parameters. If the parameters *F*, *G* and *H* are equal to 1 and *N* has the value of 3, the Hill'48 yield function will be reduced to the von Mises model. The most common method for obtaining material parameters of the Hill'48 model is based on determination of the *r*-values along 0°, 90° and 45° to the rolling direction. From Eq. 4, the anisotropic parameters *F*, *G*, *H* and *N* can be rewritten in terms of the *r*-values r_0, r_{45}, r_{90} as followed:

$$F = \frac{r_0}{r_{90}(1+r_{90})}, G = \frac{1}{(1+r_0)}, H = \frac{r_0}{(1+r_0)}, N = \frac{(r_0+r_{90})(1+2r_{45})}{2r_{90}(1+r_0)} \tag{2.8}$$

For the determination of the anisotropic parameters, uniaxial tensile tests of sheet samples prepared from different directions were performed to identify the *r*-values and the yield stress for the rolling direction, in which will be described in APPENDIX A.

2.2.1.3 Yld2000-2d Yield Criterion

In addition, a non-quadratic anisotropic yield function introduced by Barlat et al. [7] was employed to describe the anisotropic behavior of the examined steel sheets. In this model, an isotropic yield function was initially presented by the yield potential function suggested by Hosford [7] as followed:

$$\phi = \phi' + \phi'' = 2\bar{\sigma}^M \tag{2.9}$$

$$\phi = \left|S_1' - S_2'\right|^M + \left|2S_2'' + S_1''\right|^M + \left|2S_1'' + S_2''\right|^M = 2\bar{\sigma}^M \tag{2.10}$$

The S_i' and S_i'' are the principal values of the stress tensors S' and S'', which can be then expressed by:

$$\tilde{S}_{1,2} = \frac{1}{2}\left(\tilde{s}_{xx} + \tilde{s}_{yy} \pm \sqrt{(\tilde{s}_{xx} - \tilde{s}_{yy})^2 + 4\tilde{s}_{xy}^2}\right) \tag{2.11}$$

The S_{ij}' and S_{ij}'' are linear functions of the stress deviators

$$\begin{pmatrix} s_{xx}' \\ s_{yy}' \\ s_{xy}' \end{pmatrix} = \begin{bmatrix} L_{11}' & L_{12}' & 0 \\ L_{21}' & L_{22}' & 0 \\ 0 & 0 & L_{66}' \end{bmatrix} \begin{pmatrix} s_{xx} \\ s_{yy} \\ s_{xy} \end{pmatrix} \tag{2.12}$$

$$\begin{pmatrix} s_{xx}'' \\ s_{yy}'' \\ s_{xy}'' \end{pmatrix} = \begin{bmatrix} L_{11}'' & L_{12}'' & 0 \\ L_{21}'' & L_{22}'' & 0 \\ 0 & 0 & L_{66}'' \end{bmatrix} \begin{pmatrix} s_{xx} \\ s_{yy} \\ s_{xy} \end{pmatrix} \tag{2.13}$$

$$\begin{pmatrix} L'_{11} \\ L'_{12} \\ L'_{21} \\ L'_{22} \\ L'_{66} \end{pmatrix} = \begin{bmatrix} 2/3 & 0 & 0 \\ -1/3 & 0 & 0 \\ 0 & -1/3 & 0 \\ 0 & 2/3 & 0 \\ 0 & 0 & 1 \end{bmatrix} \begin{pmatrix} \alpha_1 \\ \alpha_2 \\ \alpha_7 \end{pmatrix} \tag{2.14}$$

$$\begin{pmatrix} L''_{11} \\ L''_{12} \\ L''_{21} \\ L''_{22} \\ L''_{66} \end{pmatrix} = \begin{bmatrix} -2 & 2 & 8 & -2 & 0 \\ 1 & -4 & -4 & 4 & 0 \\ 4 & -4 & -4 & 4 & 0 \\ -2 & 8 & 2 & -2 & 0 \\ 0 & 0 & 0 & 0 & 9 \end{bmatrix} \begin{pmatrix} \alpha_3 \\ \alpha_4 \\ \alpha_5 \\ \alpha_6 \\ \alpha_8 \end{pmatrix} \tag{2.15}$$

In turn, the coefficients L'_{ij} and L''_{ij} are described by relationships of a set of eight coefficients α_k, as shown in the equations (2.14) and (2.15). When an isotropic case is considered, the coefficients α_1 to α_8 will be reduced to one coefficient. All these coefficients are independent. It means that eight input data are needed for the calculation. The *r* values and yield stresses from uniaxial tensile tests for three different directions (parallel, perpendicular and 45° diagonal to the rolling direction) were used. At least two additional biaxial tests needed to be carried out in order to evaluate the remaining coefficients. For instance, a hydraulic bulge test and disk compression test could be used. The calculation procedure will be described in APPENDIX A.

2.2.2 Hardening Laws

Work hardening, or strain hardening, is an intrinsic ability of material to strengthen or harden with increasing strain level and is one of the most important properties influencing the formability of sheet metals [3]. Strain hardening of the material can be isotropic or anisotropic. The former corresponds to an expansion of the yield surface without distortion. It is completely defined by a single stress-strain curve. Any other form of hardening, such as kinematic hardening, which corresponds to the translation of the yield surface, is anisotropic. In this work, only isotropic strain hardening is discussed. Empirical plastic flow descriptions have been postulated to represent the stress-strain behaviour of metals, such as the standard hardening law as described in [8,10,11].

In this research work, three hardening laws were precisely considered, namely, the Swift, Voce model, also and modified Voce model were described in [8,9,10], respectively. The swift hardening model has been used successfully for many decades, in particular for steel and dual phase, AHS steel [10].The Swift equation [8] is given by

$$\bar{\sigma} = K\left(\bar{\varepsilon}_O + \bar{\varepsilon}_p\right)^n \tag{2.16}$$

where $\bar{\sigma}$ and $\bar{\varepsilon}_p$ are respectively the effective stress and strain. The parameters *K*, *n* and ε_o are material constants, *n* is the strain hardening exponent and *K* is the strength

coefficient. If ε_o is zero for the so-called Hollomon law [11].Oppositely, the swift hardening model does not exactly describe the behavior of all materials very well. For aluminum alloys, it is often reported that the Voce law [9], as shown below in Equation 2.14, provides a better approximation of the stress-strain data compared to the Swift law [13], since, the voce model is more saturate than swift model. Oppositely, the TRIP780 can be described the stress-strain curve by the modified Voce model, in which discounts the saturated model and prepare a better prediction than swift model as demonstrated in [10].

The Voce equation can be described by

$$\bar{\sigma} = A - B_0 e^{(-C\bar{\varepsilon}p)} \tag{2.17}$$

A, B_0 and *C* are the material constants, in which are determined by fitting the experimental determined stress-strain curves. The modified Voce equation [10] can be expressed by

$$\bar{\sigma} = A - B_0 e^{(-C\bar{\varepsilon}p)} + B_1\bar{\varepsilon}p \tag{2.18}$$

where *A*, B_0, B_1 and *C* are the material constants. These material constants could be calculated by fitting the experimentally determined stress-strain curves. However, B_1 was approximately identified in this work as a half of yield stress value for each of the investigated steels.

2.3 Formability Characterization

The ability of sheet metal to deform plastically without failure during the forming process defines the sheet metal formability. Considering industrial production, formability should be ensured first among the material characteristics. Formability is primarily limited by the occurrence of failure such as plastic flow localization or instability during the forming process. General sheet forming operations consist of a combination of the basic forming operations such as bending/unbending, plane strain stretching, biaxial stretching and drawing as schematically shown in Figure 2.11. Therefore, there is no single test which can provide an accurate indication of the formability of the material when all aspects of deformation are considered. [4]

The formability of a metal is described by its flow curve and the ductility as a measure of the forming limit. In general, the plastic behaviour is given by the yield surface and its variation with strain. In the flow curve the yield stress is represented as a function of strain ε, strain rate έ, and temperature. The formability is defined as the magnitude of the effective plastic strain, which the material can suffer without damage. Parameters which influence sheet metal formability can be divided into three groups,

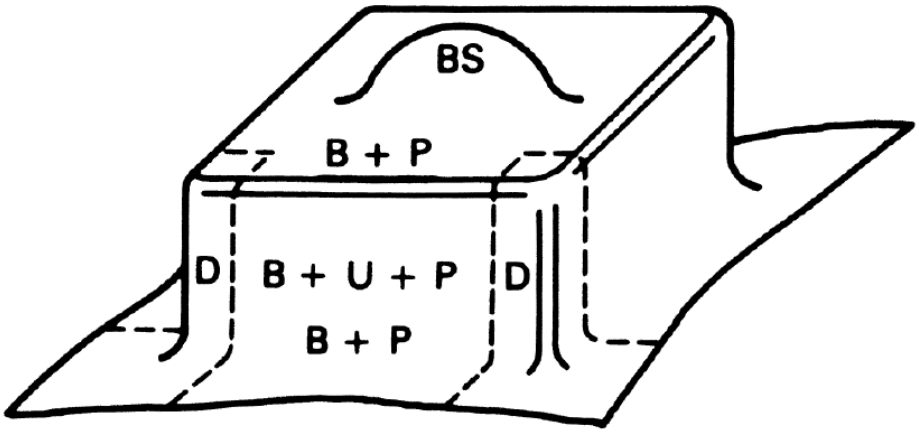

Figure 2.11 Combination of basic forming operations in the forming of a square box (B, bending; BS, biaxial stretching; D, drawing; P, plane-strain stretching; U, unbending) [4]

- Material properties including mechanical, metallurgical, and chemical properties.
- Process parameters, comprising stress state, strain rate, temperature, part configuration, and lubricant, and strain bounding criteria such as tearing, strain localisation, wrinkling, roughness, and springback. Strain localisation (necking), tearing, wrinkling, modification of the roughness or a poor appearance are factors that generally define a limit to the deformation by stretching.
- The stretching involves the forming process as bulging, hole expanding, bending, and stretch-forming. The influences of the strain boundary criterion on the formability of material by stretching and by deep drawing are illustrated in Figure 2.12. [14]

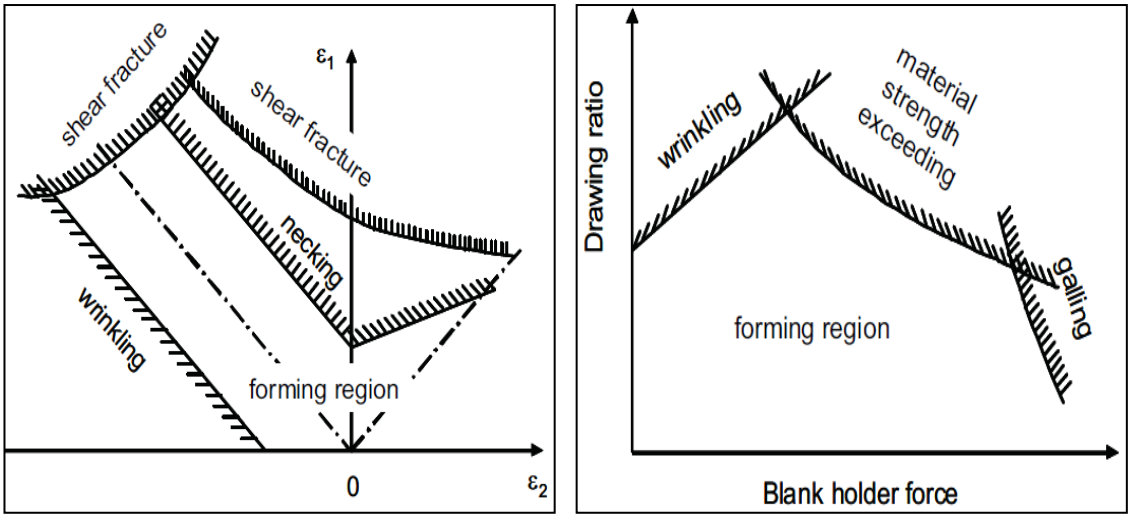

(a) (b)

Figure 2.12 Influences of various parameters on the formability in stretching (a) and deep-drawing (b) [14]

By a characterisation of formability for a forming procedure it is important to reproduce the forming history in the applied test method. Figure 2.13 shows the states of stress in different specific material formability testing. During a complex or multi-step sheet forming process a combination of various states of stress occurring in a component is possible. In this chapter only characterisation methods for sheet metal with less than 3 mm thickness are treated. [1]

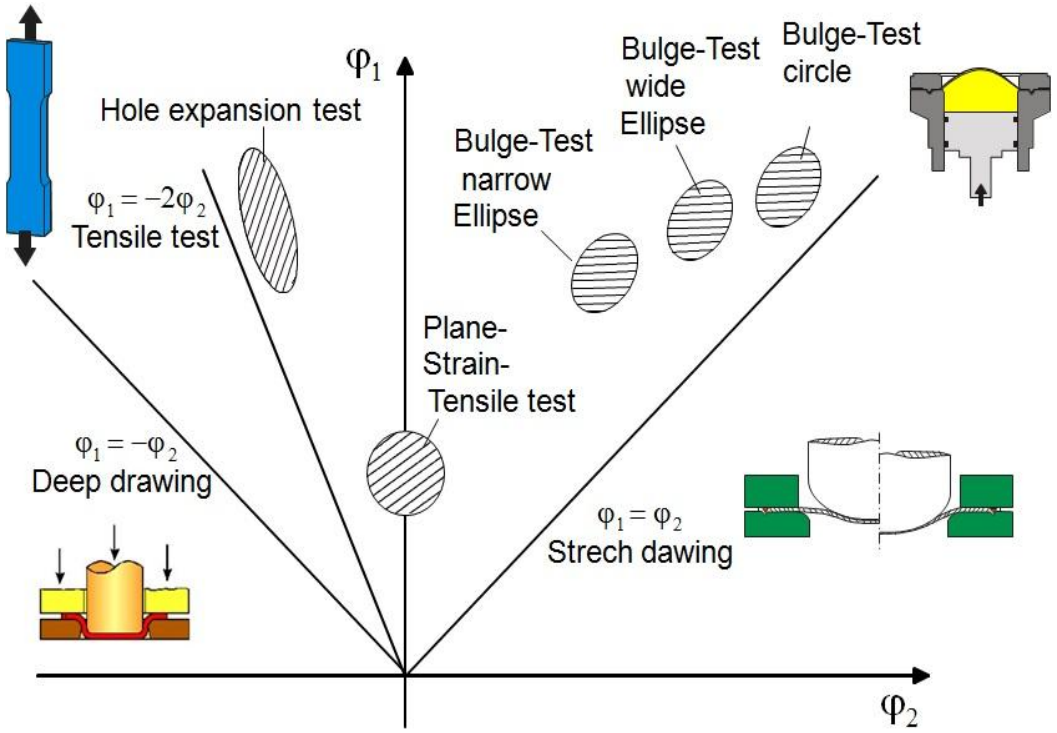

Figure 2.13 States of stress in different formability testing [1]

2.3.1 Evaluation of the Sheet Metal Formability

At the end of the nineteenth century, due to the development of the sheet forming technology, sheet metal formability became a research topic. A detailed presentation of this research can be found in [15]. Some of the first researchers interested in this field were Bessemer and Parkes, Adamson, Considere and Erichsen [15]. Since then, various method for evaluating sheet metal formability have been developed. One may subdivide them in to four classes.[15]

- Methods based on mechanical tests
- Methods based on simulating tests
- method of the limiting dome height
- methods based on forming limit diagrams

2.3.1.1 Methods Based on Mechanical Tests

This method can be called intrinsic tests, which provide the basic characteristic properties of materials. The uniaxial tension test is the most extensively used intrinsic test because it can provide many material properties such as Young's modulus, yield strength, tensile strength, uniform elongation, total elongation, strain hardening exponent, strain rate sensitivity, and r-value, which represents the material anisotropy. Consequently, the hydraulic bulge test as shown in Figure 2.14 is also widely used in

describing the strain hardening characteristics of sheet materials because the range of plastic strain is much larger than can be achieved in uniaxial tension before instability occurs [16, 17].

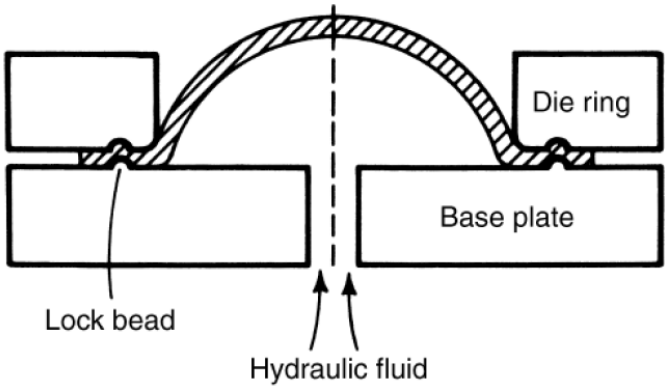

Figure 2.14 Schematic of hydraulic bulge test [18]

2.3.1.2 Methods Based on Simulating Tests

The simulative tests may be more useful and relevant than intrinsic tests to evaluate the formability of sheet parts. In simulative tests, the sheet materials can be subjected to deformation which approximates the forming operations including the factors which are not present in the intrinsic tests, such as bending/unbending and friction. The stretching tests, such as ball punch tests, have been introduced to determine the properties of sheet metals in stretching. [19]

The first test for evaluating the formability of sheet metals was proposed by Erichsen [15]. The test consists in stretching a sheet specimen by means of a hemispherical punch until the occurrence of fracture, see Figure 2.15. The depth of the punch indentation in the specimen expressed in millimetres is the so-called Erichsen index (IE). This is the most commonly used parameter for expressing the formability of sheet metals. Various researchers have analyzed the accuracy, the limits of applicability as well as the factors influenc in the test results as reported in [15]. Olsen [20] introduced a test similar to that proposed by Erichsen but with a different size of the tools. The index established using these methods has a low accuracy due to the small size of the tools, the impossibility of ensuring a sound fix in of the specimen and poor lubrication. N order to diminish these errors Hecker [21] proposed a formability test based on stretching a punch having a greater diameter than that in the Erichsen and Olsen tests. In this case the blank is also held by draw-beads whereby there is a dryfriction regime between punch and specimen. Like for the Erichsen and Olsen test the formability index is expressed by the depth of the punch indentation at the beginning of fracture. Since most of the defects in deep-drawing of complex parts are located near the region on plane stretching (plane strain), Ghosh proposed a modification of the Hecker test in the order of simulating this state of strain. For this purpose he used Hecker’ s device with strip specimens of various widths. This test, called the limit dome height test (LDH), will be described in next Section (2.3.1.3).

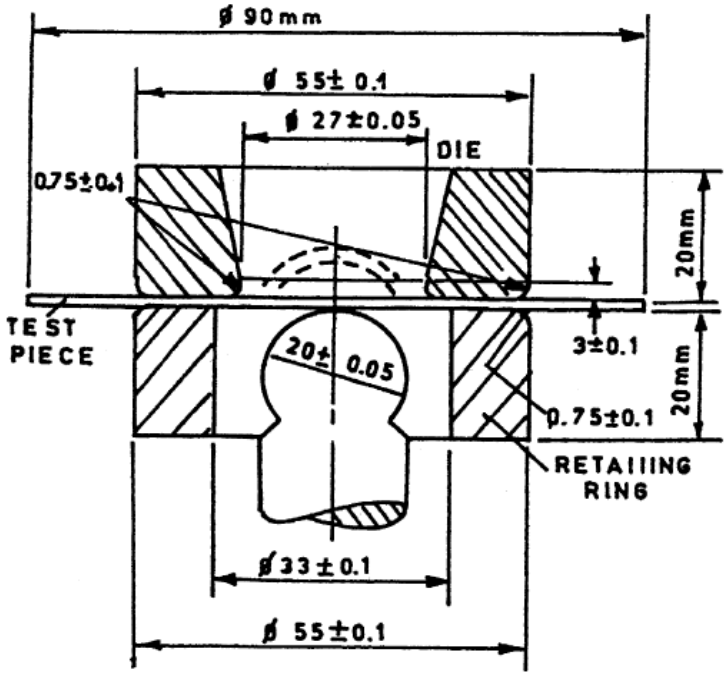

Figure 2.15 Scheme of Erichsen test

2.3.1.3 Limit Dome Height Method

This method combines advantages of simulating tests and of the forming limit diagram. Based on observations by Drewes [22], Ghosh [23] proposed to represent the heights of the parts as functions of the minimum strains occurring in rectangular specimens (of Nakazima type) stretched on a hemispherical punch until fracture. By drawing a curve through the experimental points obtained with specimens of different width, a diagram like shown in Figure 2.16 is obtained [19]. Later on, the method has been modified by English researchers under the name of Strip Stretch Test and by American researchers, named Limiting Dome Height test. The height of the part corresponding to plane strain is a formability index denoted by LDH_0. This is the minimum compared to the heights obtained for other states of strain. The width of the specimen corresponding to plane strain is a characteristic of the material. In spite of its advantages the method has been little used in industry, due to the large dispersion of the LDH_0 value s and the large amount of experimental work. More recently, Wagoner [20] introduced the OSUFT method in order to over-come the applicability limits of the LDH method. For this purpose the shape of the tools was optimized by FE simulations aiming to achieve as close as possible a state of plane strain. The results showed a reduced dispersion and good agreement with industrial practice. Also the amount of experimental work is reduced.

2.3.2 Forming Limit Diagram (FLD)

During sheet metal forming processes, it is very important to determine whether the amount of deformation at any point of the sheet exceeds the formability limit. The forming limit diagram (FLD) has been commonly used to evaluate the formability of sheet metals and diagnose production problems in the sheet metal forming processes.

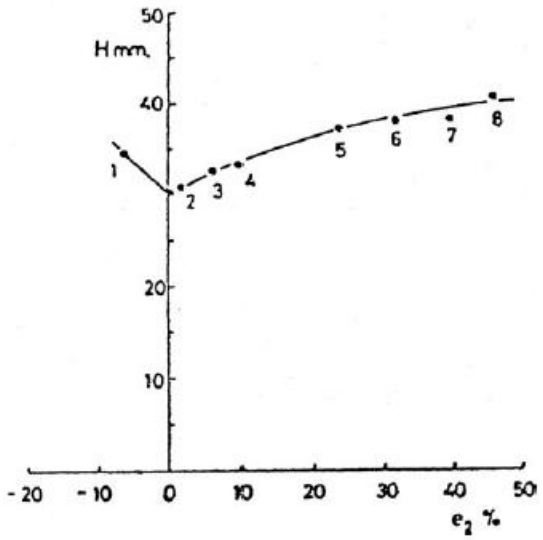

Figure 2.16 Limit dome height curve

The FLD concept was first introduced by Keeler and Goodwin as expressed in [15]. It represents the relationship between the major and minor principal strains in the surface of a sheet beyond which plastic flow localization occurs. Many attempts have been made to predict the FLD, taking into account different plasticity theories, material parameters and instability conditions. Assuming that plastic instability occurs when the load reaches a maximum value in proportional strain path, Swift [24] proposed a diffuse necking theory to calculate the limiting strains. However, in industrial stampings the maximum allowable strains are not determined by diffuse necking and, therefore, these limit curves have little practical interest. Hill [25] first described localized necking in plane stress. Hill's theory predicts localized plastic deformation in the direction of zero extension, which is only available for strain states where the minor principal strain is negative. However, since localized necking can also be observed experimentally in some biaxial stretched sheets, Marciniak and Kuczynski (M-K) [26] developed a theory based on the assumption that necking develops from a narrow band across the sheet with an initial inhomogeneity, which allows a complete description of localized necking under various plane stress states. It is well known that the MK model is sensitive to the yield surface shape and strain hardening. Therefore, many researchers combined different constitutive models with the MK analysis to predict the FLD for sheet metals. Barlat was the first to reformulate the MK model in order to take into account any anisotropic yield functions together with isotropic work hardening [13]. In his paper, the FLDs of polycrystalline aggregates were computed using yield surfaces described either by a phenomenological yield function or by the procedure of Taylor/Bishop and Hill. Paraianu et al. employed different non-quadratic yield functions to study the formability of AA3103-0. Signorelli et al. integrated the MK approach with a rate-dependant polycrystal self-consistent plasticity model to compute the FLD for two aluminum alloys. Butuc et al. applied a flexible mathematical method into the MK theory in order to develop a general code for FLD predictions in monotonic and two-stage strain paths. In this code, different yield functions and strain hardening laws can be implemented easily. Yao and Cao considered a mixed isotropic-kinematic material hardening description in the MK model and found that the forming limits were sensitive to anisotropic hardening. In addition, it is well-known that taking positive strain rate sensitivity into account shifted the FLD to higher major strain levels in better agreement

with experiments. However, in practice, failure occurs by different mechanisms which are material dependent. Moreover, it is well known that, in the strain paths near balanced biaxial stretching, fracture can occur before the onset of localized necking. In these cases, the MK model should not be used to predict the limit strains. For example, Chung et al. compared the measured FLDs of TWIP940 and DP600 steel sheets with the theoretical prediction of localized necking based on the MK model. They found that for both materials the FLD in the stretching range was extremely over predicted. [13]

2.3.2.1 Forming Limit Diagram Development Concept

The forming limit diagram is a constructive concept for characterizing the formability of sheet metal. It was proved to be an essential tool for material selection, design and try out of the tools for deep drawing operations. Since the experimental determination of FLDs requires a wide range of sheet forming tests, consequently a large variety of expensive equipment and tremendous experimental effort, many attempts have been made to predict the FLDs, taking into account the theory of plasticity, material parameters and instability conditions. The objective of this section is to review the Forming Limit Diagram concept, its experimental determination and the next section (2.4.1) will described the pertinent theoretical studies related to the analysis of forming limit diagrams (FLDs).In addition, the theories advanced toward the understanding and predicting such strains under complex loading conditions will be described of particular interest is the Marciniak - Kuckzinsky method (M-K) and its sensitivity on different factors. [12]

Stretch forming is a significant component in many sheet metal manufacturing process. Simultaneously with the progressively thinning of a sheet, two modes of plastic instability are possible, a diffuse necking follows by a localized necking. A study of failure in biaxial stretched sheets by Keeler and Backofen [27] showed the existence of what is known as forming limit diagrams (FLDs).The main discovery was that the largest principal strain before any localized thinning in a sheet increased as the degree of biaxiality increased as plotted in Figure 2.17. They had tested several material including steel, cooper, brass and aluminium sheets by stretching them over solid punches. Additionally, Keeler found the material properties have great effect on the strain distribution in biaxial stretching of sheet metal. He pointed out that for higher exponent of the material work hardening, n ,the strain distribution will be relatively homogeneous. On the contrary, materials having lower n values develop sharp strain gradients and the deformation concentrates in a very small region, then causing premature failure. A map in principal strain space $(\varepsilon_1, \varepsilon_2)$, separates safe strain states that a material could provide, from the more severe states, which would lead to failure. By definition, ε_1 is the major principle strain, and ε_2 is the minor principle strain. Therefore, FLDs show the combination of major and minor in-plane principle strain beyond which failure occurs. With further development of the experimental technique by Goodwin [28], a FLD for mild steel was obtained serving as a criterion for most stamping processes and often being referred as Keller and Goodwin diagram Figure 2.18 Due of the contribution of both authors to the understanding of material formability. [12]

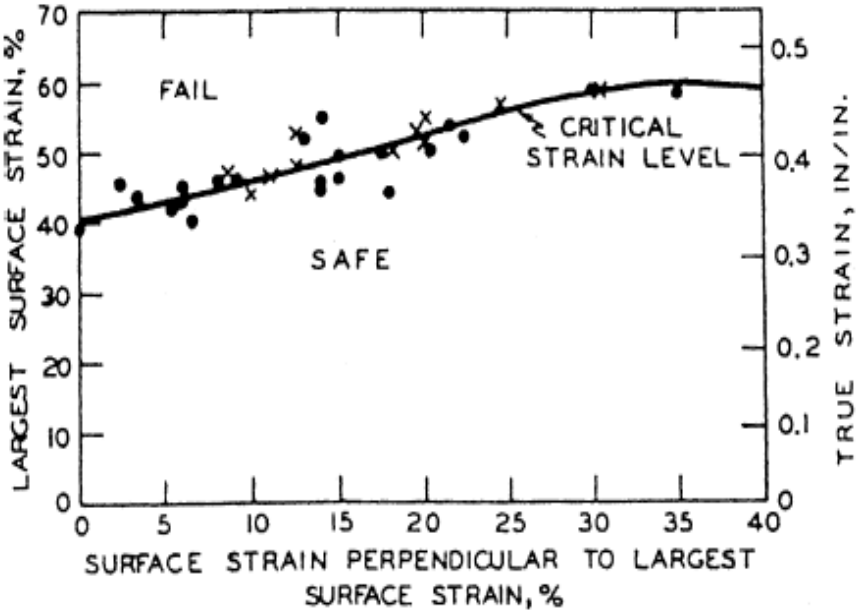

Figure 2.17 Forming limit diagram define by Keeler [15, 27]

Goodwin [28] plotted the curve for the tension/compression domain (ε_1>0; ε_2<0) by using different mechanical tests as shown in Figure 2.18. In this case, transverse compression allows for obtaining high values of tensile strains like in rolling or drawing. The diagrams of Keeler (rightside) and Goodwin (leftside) are currently called the Forming Limit Diagram (FLD), see Figure 2.18. Connecting all of the points corresponding to limit strains leads to a Forming Limit Curve (FLC). The "fail" region located above the FLC and "save" region located below the FLC. The Forming Limit Curve (FLC) is plotted on a Forming Limit Diagram (FLD).

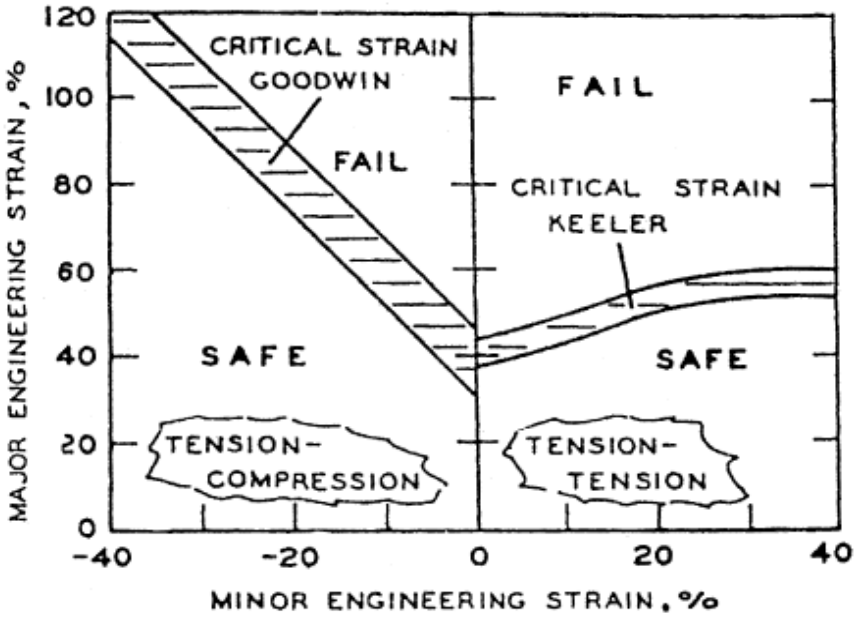

Figure 2.18 Forming limit diagrams define by Keeler and Goodwin [15]

The intersection of the limit curve with the vertical axis (which represents the plane strain deformation (ε_2=0) is an important point of the FLD and is noted FLD_0. The position of this point depends mainly on the strain hardening coefficient and also on thickness. It was well established that the formability in sheet metal forming can be evaluated by the FLD. The FLD curve can be used as indicator for the onset of necking or the fracture occurrence, depending on when and where the strains are determined, shown in Figure 2.19.

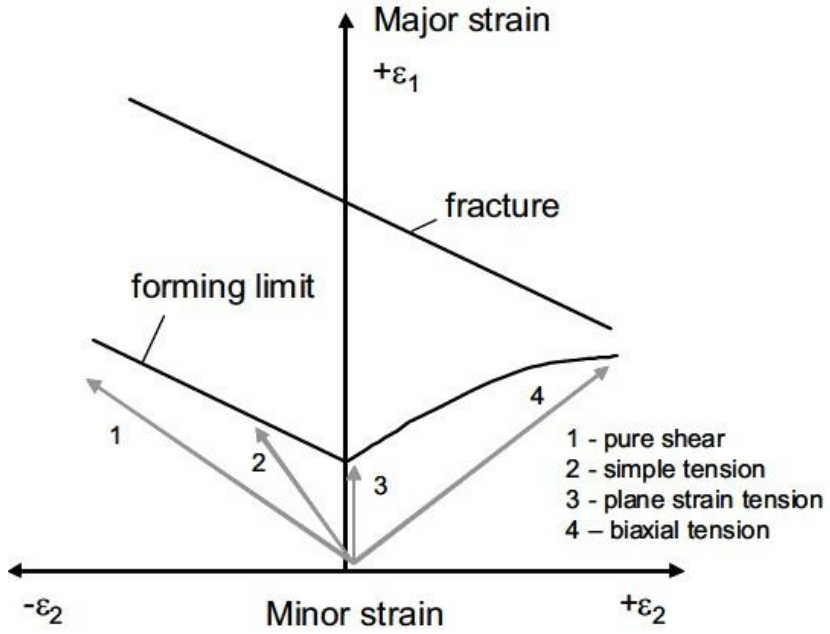

Figure 2.19 Forming limit diagrams for necking and fracture [1,15]

2.3.2.2 Experimental Determination of the FLDs [15]

FLDs must cover as much as possible the strain domain which occurs in industrial sheet metal forming processes. The diagrams are established by experiments that provide pairs of values of the limit strains ε_1 and ε_2 obtained for various loading patterns (equi-biaxial, bi-axial, uniaxial). In order to determine a FLD one must generate load paths ranging from equibiaxial tension ($\varepsilon_1 = \varepsilon_2$) to pure shear. ($\varepsilon_1 = -\varepsilon_2$). In practice the state of simple tension ($\varepsilon 1 = -2\varepsilon_2$ for isotropic materials) is never exceeded in the blankholder region. It is necessary to deform the specimen along a linear strain path, i.e. the trajectory followed by appoint in the $\varepsilon_1, \varepsilon_2$ - plane until reaching the forming limit must be a straight line.

1. Uniaxial Tensile Test

This test allows determining a section of the FLD in the range ε_2<0. For obtaining different strain paths, specimens with different shapes and sizes with and without notches are used, as depicted in Figure 2.20 [29]. The advantages of the tensile test for determining FLDs are that the specimens are easy to manufacture and a general purpose testing machine can be used, Furthermore, the specimens remain plane during the test which facilitates measurement. However, only the negative section of the forming limit diagram (ε_2<0) can be determined.

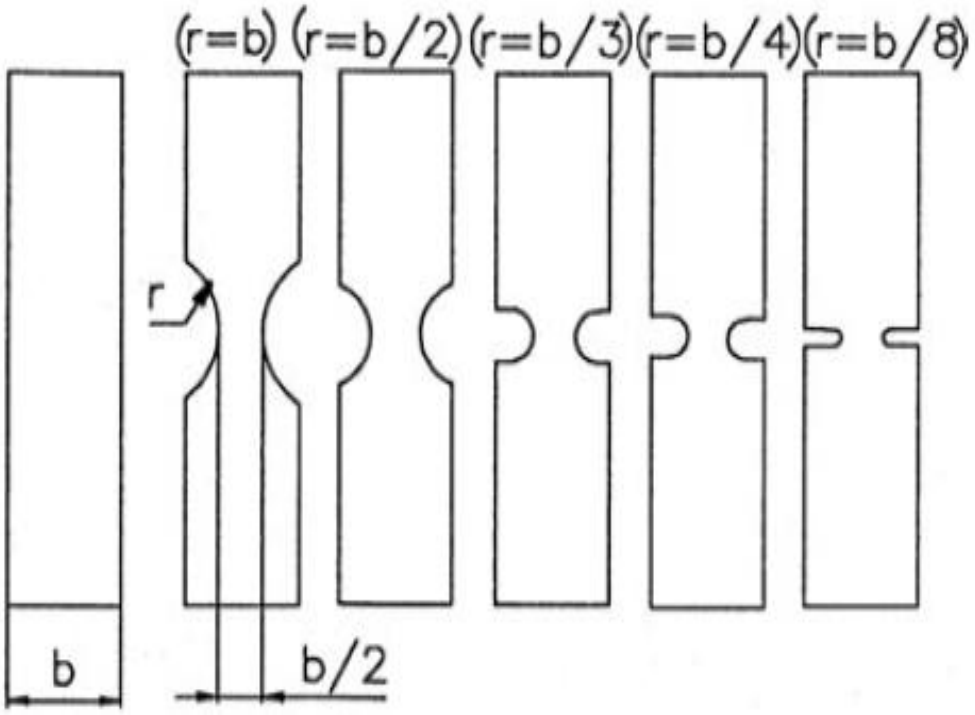

Figure 2.20 Rectangular specimens with and without notches [29]

2. Hydraulic Bulge Test

This test was first proposed by Olsen [20]. For varying the strain path elliptical dies of different shape can be used, see Figure 2.21. The most important advantage of the test is the absence of friction. The disadvantage is that only the section of the forming limit diagram for positive values of ε_2 can be obtained.

3. Punch Stretching Test

This test was first proposed and used by Keeler himself. It consists of stretching a specimen (2) clamped between a blank-holder (3) and a die (4) using a spherical of elliptical punch, see Figure 2.22.The strain path is mainly varied by using specimens of different width; is can also be varied by varying the punch radius and the lubricant. Instead of using rectangular specimens Hasek applied specimens with circular recesses.

4. Keeler Test

This test consists in the use of punches having different radii in order to vary the stress state, see Figure 2.23. Disadvantages of the test are the large amount of experimental work; only the positive section of the forming limit diagram is obtained, and the shape and position of the forming limit is influence by the punch radii.

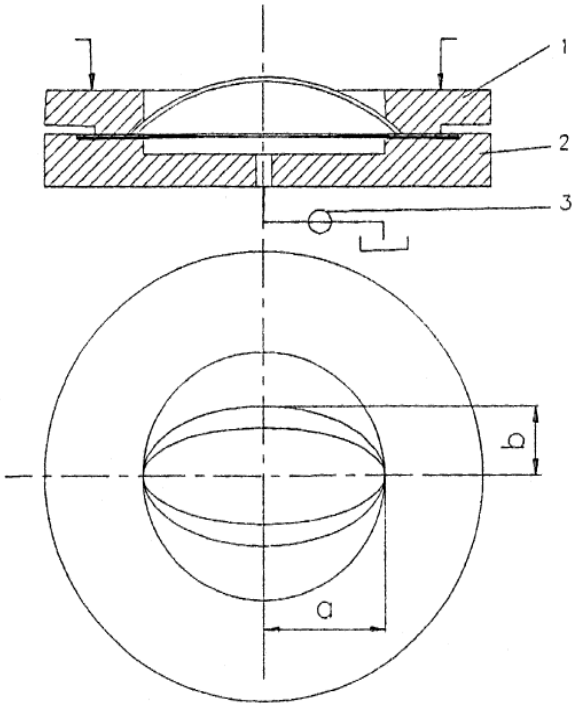

Figure 2.21 Scheme of hydraulic bulge test with elliptical dies [29]

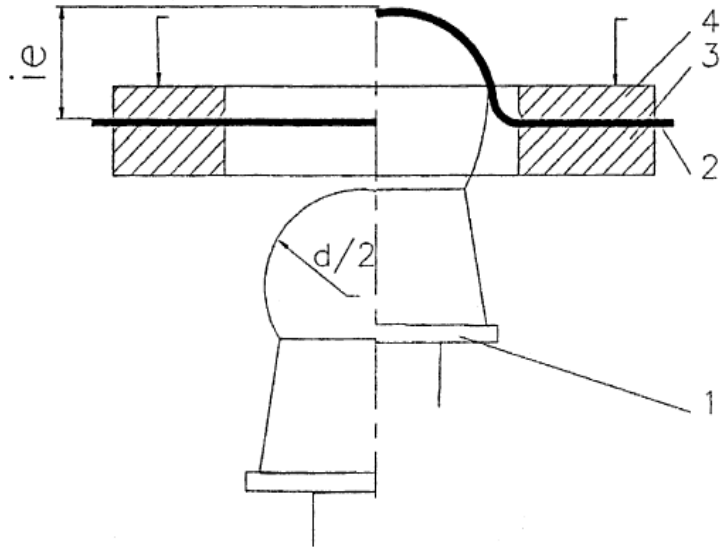

Figure 2.22 Schematic layout of the punch stretching test

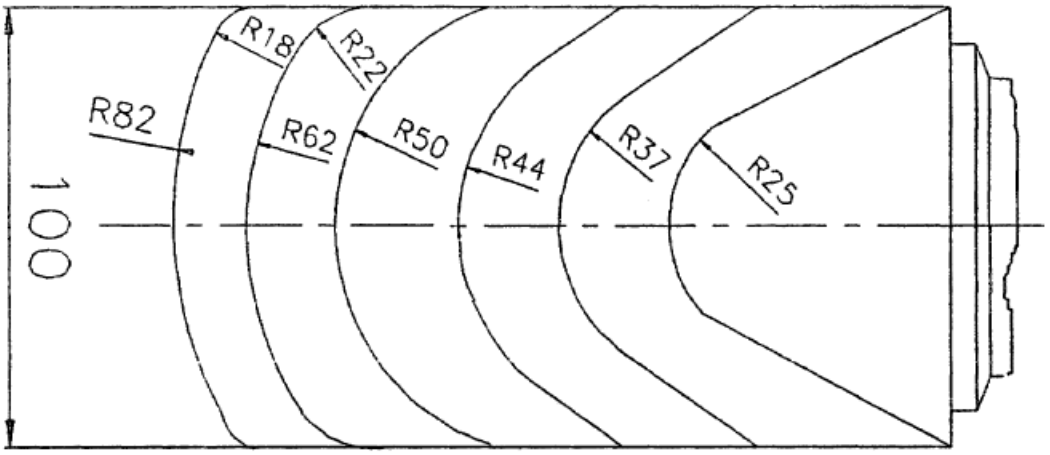

Figure 2.23 Punches used in the Keeler test

5. Marciniak Test [15]

In deepdrawing with a flat bottom punch tearing of the part usually occurs at the connection between the bottom and the cylindrical wall. In order to produce the tearing at the planar bottom of the cup, Marciniak proposed.To use a hollow punch and an intermediate part having a circular hole placed between punch and workpiece, see Figure 2.24. To obtain different strain paths are used punches with different cross sections (circular, elliptical, rectangular). The advantage of this test is that tearing appears at the planar bottom of the part thus eliminating the errors of measurement caused by a curvature. Disadvantages are the complex shapes of punch and die and the limitation of the test to the positive domain of the forming limit diagram. In order to overcome these drawbacks, the test can be modified by using specimens and intermediate parts having different shapes, see Figure 2.25. By varying the radius of the recesses the entire domain of the FLD is obtained using only one ring punch.

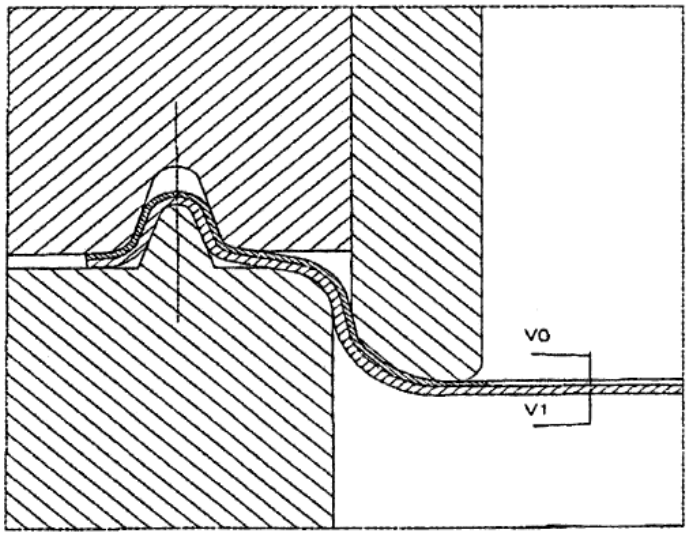

Figure 2.24 Schematic layout of the device used in the Marciniak test

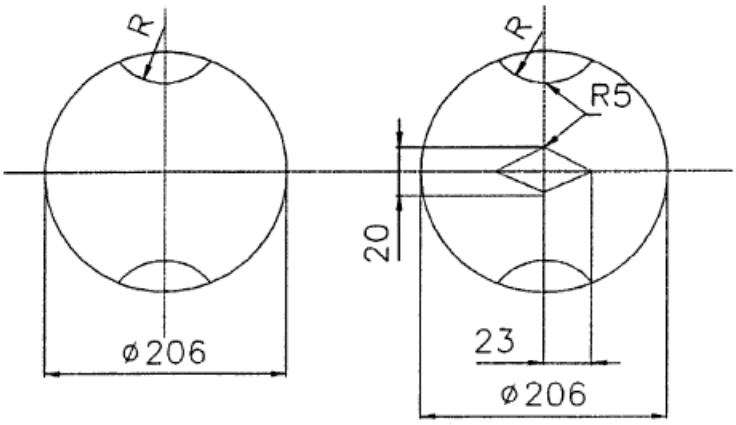

Figure 2.25 Shapes of the specimens and the intermediate part

6. Nakazima Test [15]

The test [30] consists of drawing rectangular specimens having different widths using a hemispherical punch and a circular die. By varying the width of the specimen and the lubricant one may obtain both the positive and the negative domain of the FLD. The shape of the specimen recommended by ISO12004 standard is presented in the Figure 2.26.The recommended length is longer than 25% of punch diameter. For the punch diameter and the die diameter are recommended the values 100 and 105 mm, respectively.

Advantages of the test are the simplicity of the tools, the simple shape of the specimens and the possibility of covering the entire domain of the FLDs. Disadvantages are the possibility of wrinkling and errors of measurement caused by the curvature of the punch. This method isused actually as standard method by the ISO12004 standard Metallic materials. Determination of the forming limit curves.

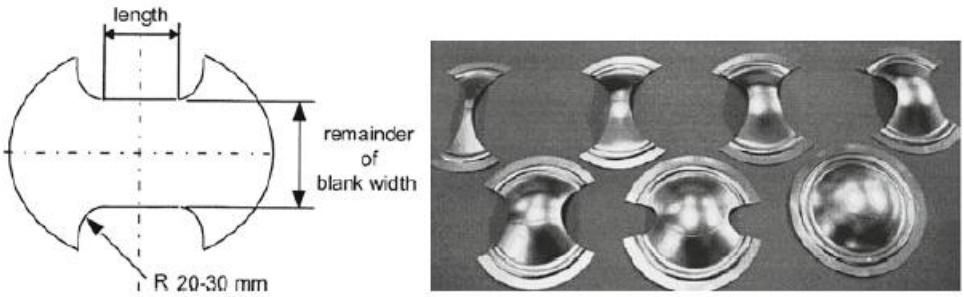

Figure 2.26 (a) Shape of the specimens used in the Nakazima test [30]
(b) the photo of a set of specimens for a complete FLD

7. Hasek Test [15]

In order to avoid wrinkling of the specimens Hasek proposed the use of circular specimens with recesses of different radii, see Figure 2.27. This requires an increase d amount of work for manufacturing the specimens.

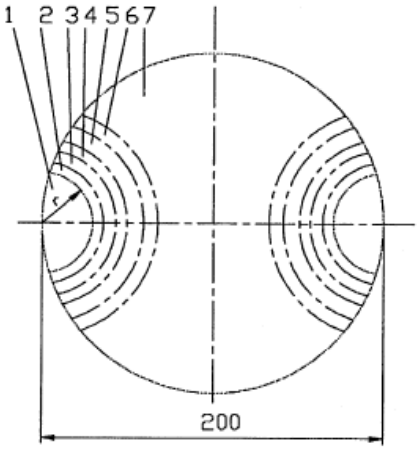

Nr.	1	2	3	4	5	6	7
r(mm)	0	4	5	57,5	65	72,5	80

Figure 2.27 Shape of the specimens used in the Hasek test

2.3.3 Theoretical Calculations of the Forming Limit Diagrams

Forming limits of sheet metals are influenced by several physical factors of which the most important ones are material work-hardening, strain rate sensitivity, plastic anisotropy, the development of structural damage and strain path. It is difficult to experimentally assess the influence of each parameter individually since it is virtually impossible to change only one at a time. The experimental determination of the forming limits in all sheet metal forming processes is not only tedious and expensive but also nearly impossible, since the strain paths of material points are quite non-linear and distinguished from each other. The theoretical analysis of plastic instability and flow localization may supply relevant information to prevent the failure on the sheet metal forming process, to examine the influence of each parameter on the necking occurrence and to improve the press performance. Therefore, an extensive effort has been devoted to the development mathematical models capable of accurately predicting the plastic flow localization of sheet metal forming processes. [12]

Various theoretical models have been developing for the calculation of forming limit curves as illustrated in Figure 2.28, which have been described to explain the localized necking in biaxial tensile fields and can be differentiated in two broad theoretical frameworks.

The first one, which is a linear method, is based on the plastic instability of homogeneous sheet metals and describes the initiation of localized band of straining in an otherwise uniform sheet, in order to obtain an explicit expression for predicting the limit strains The first ones were proposed by Swift [24] and Hill [25] assuming homogeneous sheet metals (the so-called models of diffuse necking and localized necking), respectively. The Swift model has been developed later by Hora (so-called Modified Maximum Force Criterion-MMFC) [31]. Storen and Rice [32] have been developed a model based on the bifurcation theory. Dudzinski and Molinari [33] used the method of linear perturbations for analyzing the strain localization and computing the limit strains.

The second one, which is a non-linear method,is based on the plastic instability of non-homogeneous or heterogeneous sheet metals. It is assumed an initial weakness, imperfection or inhomogeneity in the sheet, which gradually develops into neck as straining proceed. Marciniak and Kuczynski [26] proposed a model taking into account that sheet metals are heterogeneous from both the geometrical and the structural point of view. Since the theoretical models are rather complex and need a profound knowledge of continuum mechanics and mathematics while their results are not always in agreement with experiments, some semi-empirical models have been developed in recent years.[15,34]

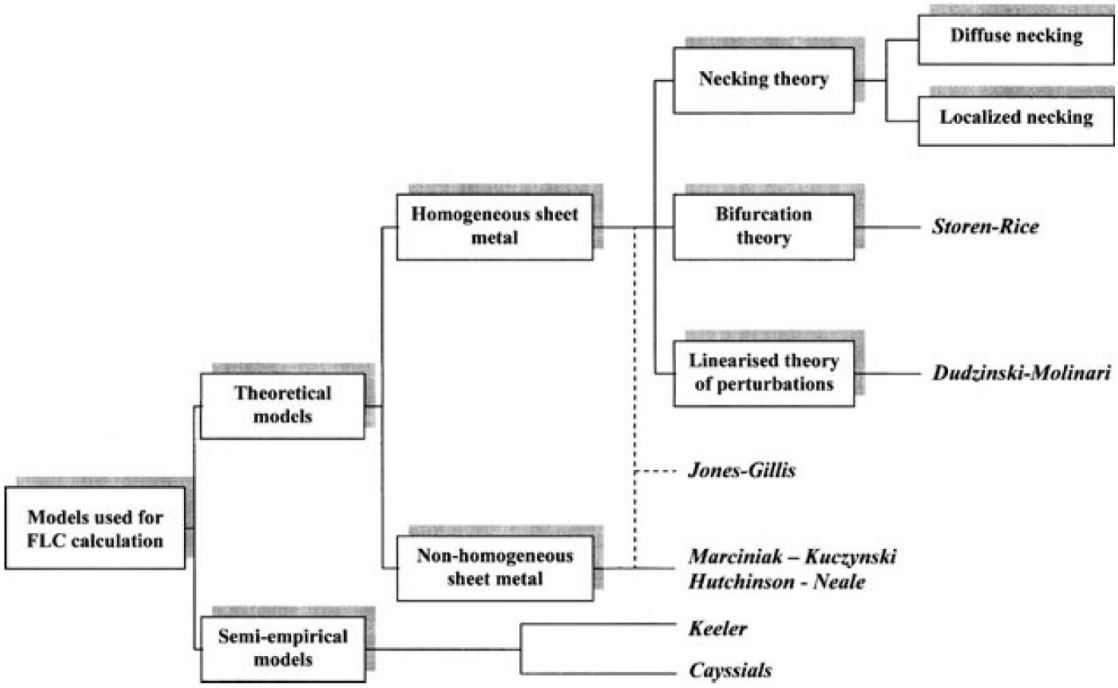

Figure 2.28 Theoretical models used in FLC calculation [15]

In the next sections the most commonly used models are presented briefly with the focus on those based on the necking phenomenon (Swift and Hill), the Marciniak–Kuczynski model, respectively.

2.3.3.1 Linear Analysis

1. Swift's Model

Considère [35] approached for the first time the problem of plastic instability in uniaxial tension. In the case of ductile materials, two domains may be distinguished in the region of plastic straining. In the first domain the hardening influence on the traction force is stronger than the influence of the cross-section reduction. This is the so-called "domain of stable plastic straining",being characterized by the fact that an increase of the traction force is needed in order to obtain an additional deformation of the specimen. In the second domain material hardening cannot compensate the decrease of the traction force due to the reduction of the specimen's cross-section. This is the so-called "domain of unstable plastic straining", being characterized by a decrease of the traction force, although the stress continues to increase. The beginning of necking corresponds to the maximum of the traction force. From the mathematical point of view, this condition can be written in the form. [15]

$$dF = 0 \tag{2.19}$$

By simple mathematical manipulations the following condition of plastic instability is obtain

$$\frac{d\sigma}{d\varepsilon} = 1 + \sigma \tag{2.20}$$

Assuming a Ludwik-Hollomon strain hardening law,

$$\sigma = K\bar{\varepsilon}^{n} \tag{2.21}$$

Then the condition (2.20) becomes

$$\bar{\varepsilon} = n \tag{2.22}$$

Hence, according to Considère 's criterion, a material obeying the Ludwick-Hollomon hardening law starts to neck when the strain is equal to the hardening coefficient.

In 1952, Swift [24] used the Considère criterion in order to determine the limit strains in biaxial tension. He analyzed a sheet element loaded along two perpendicular directions and applied the Considère criterion for each direction. Assuming a strain hardening described by Equation 2.21, he obtained the following expressions for the limit strains. [15]

$$\varepsilon_1^* = \frac{\sigma_1\left(\frac{\partial f}{\partial \sigma_1}\right)^2 + \sigma_2\left(\frac{\partial f}{\partial \sigma_2}\right)\left(\frac{\partial f}{\partial \sigma_1}\right)}{\sigma_1\left(\frac{\partial f}{\partial \sigma_1}\right)^2 + \sigma_2\left(\frac{\partial f}{\partial \sigma_2}\right)^2}.n \tag{2.23}$$

$$\varepsilon_2^* = \frac{\sigma_2\left(\frac{\partial f}{\partial \sigma_1}\right)^2 + \sigma_1\left(\frac{\partial f}{\partial \sigma_1}\right)\left(\frac{\partial f}{\partial \sigma_2}\right)}{\sigma_1\left(\frac{\partial f}{\partial \sigma_1}\right)^2 + \sigma_2\left(\frac{\partial f}{\partial \sigma_2}\right)^2}.n \tag{2.24}$$

Where *f* is the yield function. By using different yield functions, it is possible to evaluate the limits trains as functions of the loading ratio α and the mathematical parameters of the material (hardening coefficient *n*, anisotropy coefficient *r*, strain-rate sensitivity *m*,).

As an example, if the Hill 1948 criterion is used, the limit strains are as follows

$$\varepsilon_1^* = \frac{[1+r(1-\alpha)]+\left(1-\frac{2r}{1+r}\alpha+\alpha^2\right)}{(1+r)(1+\alpha)\left[1-\frac{1+4r+2r^2}{(1+r)^2}\alpha+\alpha^2\right]}.n \tag{2.25}$$

$$\varepsilon_2^* = \frac{[(1+r).\alpha-r]+\left(1-\frac{2r}{1+r}\alpha+\alpha^2\right)}{(1+r)(1+\alpha)\left[1-\frac{1+4r+2r^2}{(1+r)^2}\alpha+\alpha^2\right]}.n \tag{2.26}$$

By computing the values of ε_1^* and ε_2^* for different loading ratios α and recording them in a rectangular coordinate system ε_1 , ε_2 the necking limit curve is obtain.[15]

2. Hill'sModel [15]

In the case of uniaxial tension, the localized necking develops along a direction, which is inclined with respect to the loading direction. Hill assumed that the necking direction is coincident with the direction of zero-elongation and thus the straining in the necking region is due only to the sheet thinning. The method used for obtaining the limit strains in this case is presented in [15].The expressions of these strains are as follows:

$$\varepsilon_1^* = \frac{\frac{\partial f}{\partial \sigma_1}}{\frac{\partial f}{\partial \sigma_1}+\frac{\partial f}{\partial \sigma_2}}.n \tag{2.27}$$

$$\varepsilon_2^* = \frac{\frac{\partial f}{\partial \sigma_2}}{\frac{\partial f}{\partial \sigma_1}+\frac{\partial f}{\partial \sigma_2}}.n \tag{2.28}$$

It can be seen that

$$\varepsilon_1^* + \varepsilon_2^* = n \tag{2.29}$$

This is the Equation of a line parallel with the second bisection of the rectangular coordinate system ε_1 , ε_2 and intersecting the vertical axis at the point (0,n).According to Equation 2.29, the FLC computed on the basis of the Hill's model does not depend on the yield criterion, but only on the value of the hardening coefficient.

3. Swift and Hill's model (strain ratio)

Many sheet forming operations involve biaxial stretching in the plane of the sheet. Failures occur by the formation of a sharp local neck. Diffuse necking of sheet specimens concerns contraction in both the lateral and width directions. While localized necking leads to a specimen thinning without further width contraction. In tensile test sheet sample is elongated uniformly until reaching the maximum load, then a diffuse neck forms by contraction of both the width and thickness. A local neck develops after.

Under a general stress state of biaxial tension, the criterion for localized necking developed by Hill [25] can be expressed with the assumption of the constant strain ratio $\rho = \varepsilon_2 / \varepsilon_1$ by

$$\frac{d\sigma_1}{\sigma_1} = (1+\rho).d\varepsilon_1 \tag{2.30}$$

With power-law hardening the critical strain for local necking is then given by

$$\overset{*}{\varepsilon}_1 = \left(\frac{n}{1+p} \right) \tag{2.31}$$

n is the strain hardening exponent. According to this equation the critical strain for localised necking decreases from 2n in uniaxial tension to n for plane-strain tension [36]. The left-hand side of the FLD, i.e. the negative minor in-plane strain region may be described by this criterion. Swift reported that diffuse necking can be expected when

$$\overset{*}{\varepsilon}_1 = \left(\frac{2n.\left(1+\rho+\rho^2\right)}{(p+1).(2\rho^2-\rho+2)} \right) \tag{2.32}$$

This Swift criterion can be used for the values of the right-hand side of the FLD, however, with some underestimation. The Hill criterion shows that local neck cannot form if ε_2 is positive. Nevertheless, this is valid only when ρ and $(\alpha = \sigma_2 / \sigma_1)$ remain constant during loading. If the strain or stress path changes during stretching, local necking can occur even in the positive minor strain region. [1]

It was well established that the formability in sheet metal forming can be evaluated by the FLD. The FLD curve can be used as indicator for the onset of necking or the fracture occurrence, depending on when and where the strains are determined, shown in Figure 2.29. Figure 2.29 is a comparison of an experimental FLD with the criterion mentioned above for localized and diffuse necking. For the negative ε_2, the experimental and the theoretical curves are parallel.The experimental curve is higher, since a neck may be developed before it can be detected. In order to determine a FLD load paths ranging from equibiaxial tension $(\varepsilon_1 = \varepsilon_2)$ to pure shear $(\varepsilon_1 = -\varepsilon_2)$ must be generated.The most frequently applied method for determination of the FLD diagram is the Nakazima test [37]. In this test drawing rectangular specimens having different widths, a hemispherical punch, and a circular die are used. By varying the width of the specimen both the positive and negative domain of the FLD can be obtained. The detail of the FLD determination by the Nakazima test using an optic strain measurement will be given in the next chapter.

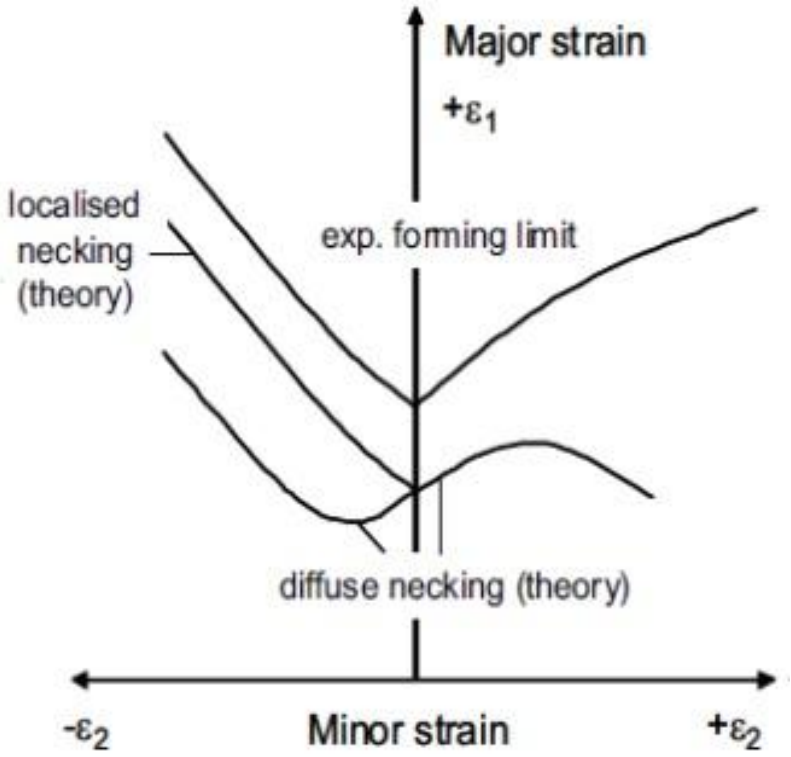

Figure 2.29 Experimental and Theoretical Determined FLD of Necking Criterion [15]

The level of the FLD increases with the sheet thickness. Along a linear strain path the rise of the FLD level is proportional to the increase of thickness. The size of the initial grid has also influence on the FLD. When determining the FLD for necking, the strain gradients are rather low. However, when determining the FLD for fracture, higher strain gradients occur. Thus, a smaller grid size must be used to improve the resolution. In general, uniform and ultimate elongation of a material rise by increasing of the strain hardening exponent n. This effect leads to a higher FLD curve. In the range of expansion $(\varepsilon_1 > 0; \varepsilon_2 > 0)$ with the increase of n, the corresponding FLD is shifted to the right i.e. to the higher values of equivalent strain. [1]

2.3.3.2 Marciniak- Kuczynski Method

According to the theory of Marciniak and Kuczynski (MK) [26], plastic instability in the sheet is studied using a two-region model in which a thickness non-homogeneity, i.e., a surface groove b, is inclined at an angle Ψ_0 to the minor principal strain direction, as shown in Figure 2.30. The axes 1, 2 and 3 present the major and minor strain directions, and the normal direction (ND) of the sheet, respectively. In addition, the initial imperfection is defined as $f_0 = e_0^b / e_0^a$, which is the ratio of the thicknesses in the two regions. A stress state is imposed on the homogeneous region a and remains constant during the deformation. The evolution of the strain rates in both regions a and b is calculated until plastic flow localization occurs in region b.

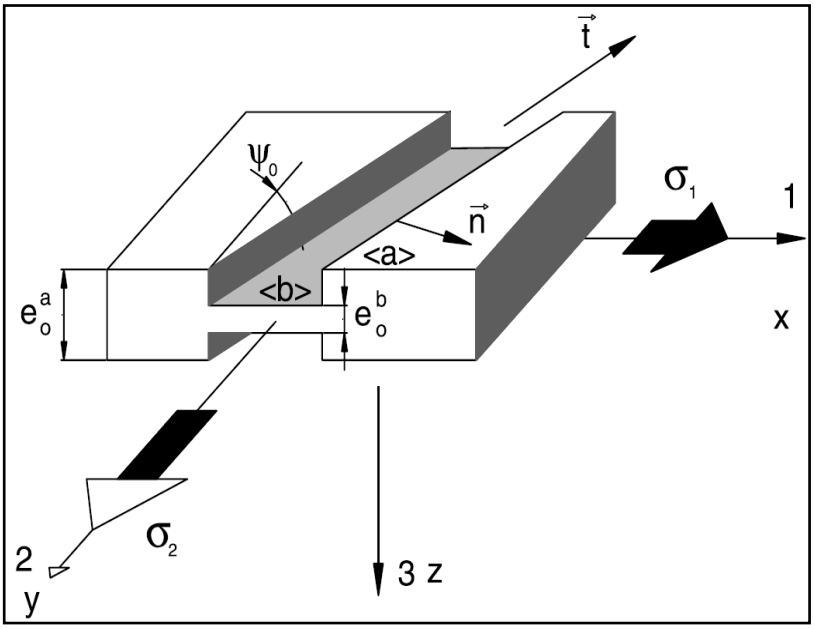

Figure 2.30 Schematic illustration of localized necking in the MK model [26]

The isotropic work hardening assumption for plane stress leads to Equation 2.26.

$$\bar{\sigma}d\bar{\varepsilon} = \sigma_{11}d\varepsilon_{11}\left(1+\alpha\rho+2\beta\gamma\right) \tag{2.33}$$

in both regions, where

$$\alpha = \sigma_{22}/\sigma_{11}, \rho = d\varepsilon_{22}/d\varepsilon_{11}, \beta = \sigma_{12}/\sigma_{11}, \gamma = d\varepsilon_{12}/d\varepsilon_{11} \tag{2.34}$$

The stress state is defined by α and β. Since the yield function should be convex and the associated flow rule is considered, ρ and γ are uniquely determined from α and β. It is worth mentioning that, for region a there is no in-plane shear stress if the major strains are aligned with the material symmetry axes. For region b, a shear stress generally exists due to the groove orientation.

The force equilibrium conditions of the sheet element with a localized necking can be written in the groove coordinate system as

$$\sigma^a_{nn}.\mathrm{e}^a_0 = \sigma^b_{nn}.\mathrm{e}^b_0 \tag{2.35}$$

$$\sigma^a_{nt}.\mathrm{e}^a_0 = \sigma^b_{nt}.\mathrm{e}^b_0 \tag{2.36}$$

In Equations 2.35 and (2.36), n and t denote the normal and tangential directions, respectively, to the current groove orientation. The superscripts *a* and *b* refer to regions *a* and *b* of the sheet, see Figure 2.30.

The compatibility condition which states that the strain in the tangential direction to the groove is the same in both regions can be expressed by Equation 2.37

$$d\varepsilon_{tt}^{a} = d\varepsilon_{tt}^{b} \tag{2.37}$$

The rotation of the groove during plastic deformation is given by Equation 2.38

$$\tan(\varphi + d\varphi) = \tan\left(\frac{1+d\varepsilon_{11}^{a}}{1+d\varepsilon_{22}^{a}}\right) \tag{2.38}$$

It is also assumed that, during plastic deformation, the material is incompressible. Then in both regions:

$$d\varepsilon_{11} + d\varepsilon_{22} + d\varepsilon_{22} = 0 \tag{2.39}$$

The solution of these equations is obtained by numerical iteration. First, the effective strain in the homogeneous region $d\bar{\varepsilon}^{a}$ is imposed and the step size is set to 0.001. Therefore, all stresses and strains in region a, are known. With stress and strain tensor transformations from the groove coordinate system to that of the material, Equations (2.35), (2.36) and (2.37) express the relationship between α^{b}, β^{b} and $d\bar{\varepsilon}^{b}$. The stresses and strains in region b are obtained by solving these three equations. Then a new increment $d\bar{\varepsilon}^{a}$ is given. When the ratio of $d\bar{\varepsilon}^{a}/d\bar{\varepsilon}^{b}$ tends towards zero (practically, less than 0.1), necking instability and strain localization are assumed to occur. The corresponding strains ε_{11}^{a} and ε_{22}^{a} are the limit strains in the current stress state

2.3.4 Forming Limit Stress Diagram (FLSD)

2.3.4.1 Forming Limit Stress Diagram Development Concept [1]

The conventional forming limit diagram (FLD) is a well accepted tool for predicting the formability and the safety limit of a material in sheet metal forming industry with respect to the development of a localised neck prior to fracture. The FLD is a strain based failure criterion, which describes the transition from safe material behaviour to material failure. In fact, the determination of the FLD is based on the assumption of a linear or quasi-linear strain path $(d\varphi_2/d\varphi_1 \approx \text{const.})$. A FLD for pre-deformed materials is influenced by the interactions between different states of stress. In this case, a qualitative agreement with the shape of the FLD curve for a material without pre-deformation $(d\varphi_2/d\varphi_1 \approx \text{const.})$ can be found, however, with a higher or lower formability. For example, the FLD curve shifts to higher φ_1-values when a plane stretch forming $(d\varphi_2/d\varphi_1 = \text{const.})$ follows after uniaxial tensile loading $(d\varphi_2/d\varphi_1 = -1/2)$ or after deep drawing loading $(d\varphi_2/d\varphi_1 = -1)$. On the other hand, if the stretch forming is followed by deep drawing, the FLD curve shifts to lower φ_1-values. This effect is outlined in Figure 2.31 (a).

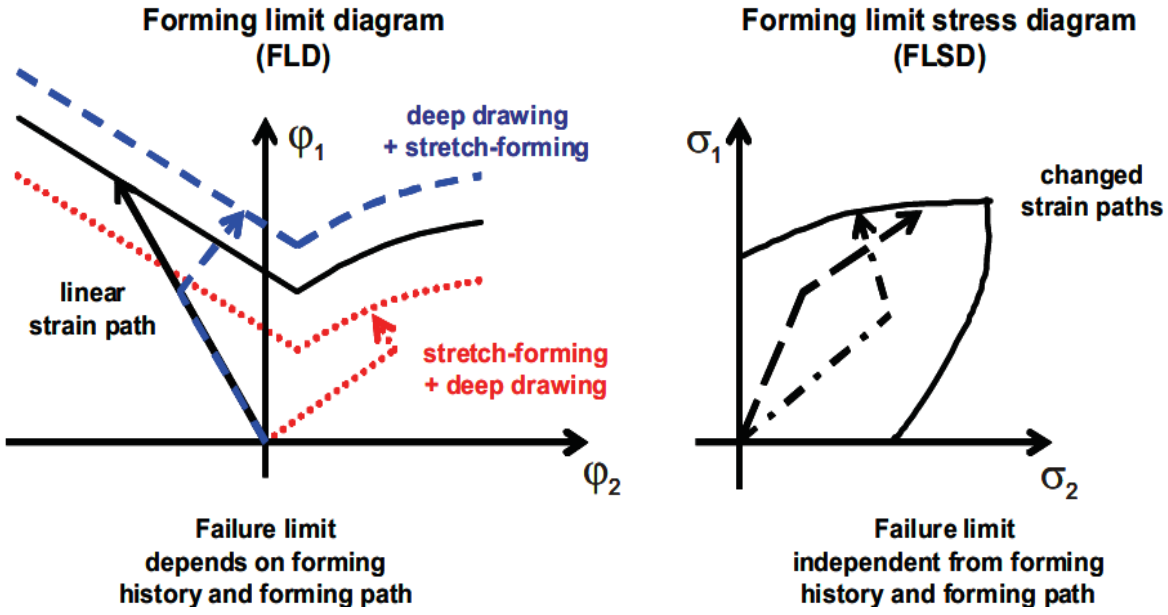

Figure 2.31 Forming limit diagram FLD and forming limit stress diagram FLSD [1]

In an industrial application, complex work pieces are usually manufactured in multi-step processes, from which the influence of the non-proportional strain history on the FLD can be problematic. Furthermore, the path is often found to be nonlinear in localized critical areas [38]. Under such conditions, the FLD cannot be used to predict whether this manufacturing will be successful or a failure. The forming limit stress diagram (FLSD) was firstly introduced by Arrieux [39, 40] in several investigations as a new failure criterion formulated by the principal in-plane stresses. It was reported that the stress based criterion or the FLSD is more robust against any changes of strain path occurring in a forming process.Since stress values cannot be determined directly in the Nakazima experiments, calculation of plastic deformation is needed. Based on the experimental forming limit strains and plasticity theory coupled with a yield criterion, the forming limit stress curves are computed.

A brief description of the proposed equations for calculating the stress values are presented here. It was assumed that the principal anisotropy axes of orthotropic symmetry are coincident with the principal stress axes. The strain path is thus characterized by the strain ratio. For a more detailed description see in chapter 4.

$$\rho = \frac{\varepsilon_2}{\varepsilon_1} \tag{2.40}$$

and the stress ratio

$$\alpha = \frac{\sigma_2}{\sigma_1} \tag{2.41}$$

For materials with in-plane isotropy and by the absence of shear stress in a coordinate system aligning with the anisotropy axes, the major and minor true stresses can be expressed as followed:

$$\sigma_1 = \frac{\bar{\sigma}(\bar{\varepsilon})}{\xi(\alpha)} \tag{2.42}$$

$$\sigma_2 = \alpha\sigma_1 \tag{2.43}$$

Where $\bar{\sigma}(\bar{\varepsilon})$ represents the effective stress computed through a hardening law and $\xi(\alpha)$ is a function of material parameters α derived from the applied yield criteria. Thus, the forming limit stress curve determined from the experimental limit strains basically depends on the shape of the yield surface as well as the hardening law used to describe plastic deformation of the material. [41]

2.3.4.2 Determination of Forming Limit Stress Diagram

In this research work, the determined FLSDs are divided as three calculation methods for AHS steels, DP780, TRIP780 and JAC780Y as expressed follow

Calculation of plastic deformation based on utilization.

1. The experimentally determined FLCs data

- Calculated plastic flow behavior based on Swift and Modified Voce model.
- Coupled with various yield functions,von Mises, Hill'48 and Yld2000-2d.
- Regarded on using the experimental FLCs data.

2. The theoretically determined FLCs obtained by M-K model

- Calculated plastic flow behavior based on Swift and Modified Voce model.
- Coupled with various yield functions, von Mises, Hill'48 and Yld2000-2d.
- Corresponding the calculated FLCs obtained by M-K model.

3. The numerically determined FLCs obtained by FE simulation of Nakazima test

- Simulated FE model for Nakazima strip tests combined with plastic flow behavior based on Swift and Modified Voce model.
- Coupled with various yield functions, von Mises, Hill'48 and Yld2000-2d
- Used the experimental FLCs as failure criterion in simulation model.

2.3.5 Hydraulic Bulge Test [1, 42]

Flow curves of sheet material are usually determined by uniaxial tensile test. The region of necking on sheet specimens cannot be measured with sufficient accuracy. Thus, the flow curves can only be evaluated by tensile tests in the range below uniform elongation. With respect to typical steels in the automotive sector, it means restricted information concerning the low deformation degree. One possibility for the determination of flow curve under biaxial stress conditions is the hydraulic bulge test. In the hydraulic bulge test a circular specimen is clamped along its circumference and deformed by hydraulic pressure, as depicted in Figure 2.32. The forming process is frictionless as no punch is used. Due to the normal anisotropy of material the obtained flow curves may be deviate from those obtained by tensile tests. Much higher strains are possible in the hydraulic bulge test than in tensile test, so the effective stress-strain relations can be evaluated at higher deformations. To understand the obtained stress-strain response, a more expressed in next chapter.

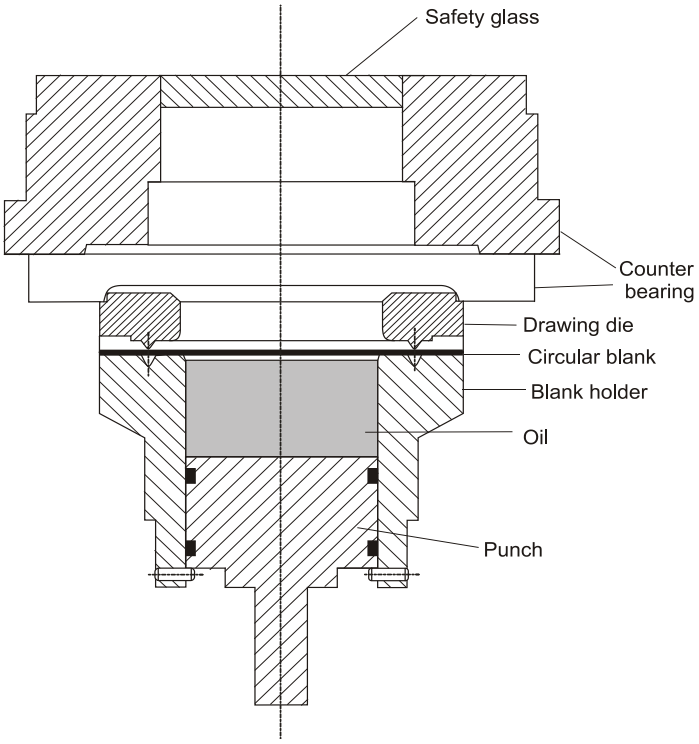

Figure 2.32 Test set-up for hydraulic bulge test [42]

Flow curves determined by tensile test and hydraulic bulge test are compared for AHS steel grades, DP780, TRIP780 and JAC780Y in Figure 3.10 and Figure 3.17-3.18. It can be clearly seen that the flow curves are in good agreement for the region of low strains. The bulge test provided flow curves up to very higher strains. It was evidenced that the results from bulge test is reproducible.

2.3.6 Hole Expansion Test [1,42]

Hole flanging is widely used for producing thin sheet components with a smoothly rounded-lip for subsequently assembly with other components. By the hole flanging, a multi loading with tangential tensile and radial compressive stress arises. Deformation mode at the edge of the hole is a combination of bending and stretching. Therefore, the conventional approaches based on tensile instability are not always sufficient to describe the hole flangeability. Hole expanding test is one of the indispensable technological formability testing which can represent the state of stress in the hole flanging process. In the hole expanding test, a round sheet sample with a blanked or machined hole in the middle is pressed by a punch, as shown in Figure 2.33. The geometry of the punch can be conical with different angles, spherical or flat. The test is interrupted when a crack initiation is detected. At the end of the test the averaged diameter of the hole at failure was measured to calculate the hole expansion ratio, which is generally utilized to specify the limitation of formability of blanks in the hole flanging process. The hole expansion ratio is defined as

$$\text{HER}=\left(\frac{D_f - D_0}{D_0}\right)\times 100\% \tag{2.44}$$

D_0 is the initial diameter and D_f is the diameter at failure of the hole.

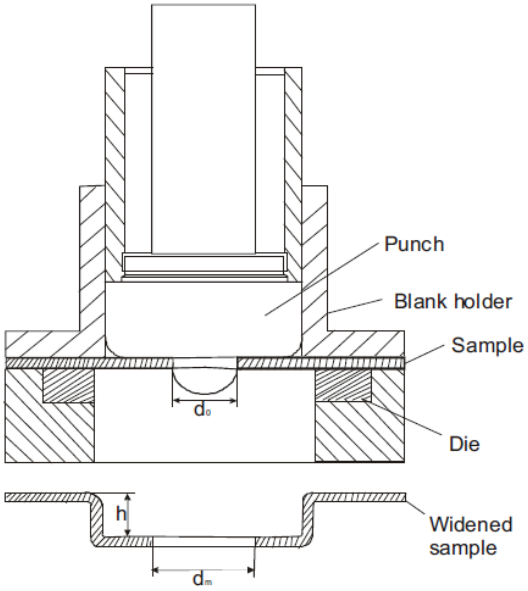

Figure 2.33 Schematic set-up of a hole expanding test

It was found that the influences of the punch profiles on the limitation of formability and cracking formation in the hole flanging process is small, however, much more on the finished shape and maximum punch load. In [43] the flangeability of different high strength steels were investigated and compared to each other with regard to localized necking and crack occurrence. Fracture during hole flanging is mainly caused by lip fracture resulted from multiple localized necking. This necking takes place around the hole periphery where straining is most severe. Some researchers used ductile fracture criteria, applied in finite element method of the stretch flange forming to study and predict the flangeability, for instance for mild and high strength steel sheets, as conducted by Takuda et al. [44]. Here, a parametric study was performed to consider the effect of void nucleation strain on the predicted onset of ductile fracture. Chatterjee et al. [45] evidenced that for multiphase steels the ultimate tensile strength is of overwhelming importance in determining the hole expansion ratio, and hence the stretch-flangeability. In contrast, the uniform elongation should not be used in analysing the ratio. Existence of some amounts of bainite in a ferritic matrix seems to be greatly advantageous for the stretch flangeability. Experimental and numerical evaluation of hole flangeability of steel sheet with respect to the hole processing conditions were carried out by Lee et al. [46]. Hole expansion ratio of steel sheets in reaming condition has much higher value than that in punching condition.

2.4 Damage criteria

The developed damage criteria were based on the micro–mechanisms of ductile fracture. Damage evolution during plastic deformation was controlled by void growth, which was in turn strongly dependent on the hydrostatic stress, as described by McClintock [47] and Rice and Tracey [48]. Atkins [49] stated that a criterion for crack initiation should be evaluated with regard to the hydrostatic stress. In Bao and Wierzbicki [50], different fracture mechanisms were observed relating to the magnitude of stress triaxialities. During deformation of metals, plastic flow can be described by the effective stress $\bar{\sigma}$, which is proportional to the root–mean square of the principal shear stress, as expressed by Equation 2.45.

$$\bar{\sigma} = \sqrt{\frac{1}{2} \times \left[\left(\sigma_1 - \sigma_2\right)^2 + \left(\sigma_2 - \sigma_3\right)^2 + \left(\sigma_3 - \sigma_1\right)^2 \right]}. \tag{2.45}$$

σ_1, σ_2 and σ_3 are the principal stresses. The hydrostatic stress σ_m is responsible for a volume increase of cavities in a porous matrix. The hydrostatic stress is the first invariant of stress tensor and does not contribute to the plastic deformation state. It depends only on the deviatoric stress, whether a state of stress causes the plastic flow. Both $\bar{\sigma}$ and $\bar{\varepsilon}$ are not affected by the hydrostatic stress. A single dimensionless parameter η, which characterizes a stress–state and is a measure of the stress triaxiality, is defined as

$$\eta = \frac{\sigma_m}{\bar{\sigma}} = \frac{\frac{1}{3}\left(\sigma_1 + \sigma_2 + \sigma_3\right)}{\bar{\sigma}} \tag{2.46}$$

Effective plastic strain to fracture is a proper measure for material ductility, which exhibits the ability of material to accept large amount of plastic deformation without suffering fracture. In Hancock and Mackenzie [51] and Bao and Wierzbicki [50], various tensile tests on notched samples were conducted. It was found that the effective strain at fracture significantly depended on the stress triaxiality value. The effective plastic strain is proportional to the root–mean square of the principal plastic strains ε_1, ε_2 and ε_3, as given by

$$\bar{\varepsilon} = \sqrt{\frac{2}{3} \times \left(\varepsilon_1^{\,2} + \varepsilon_2^{\,2} + \varepsilon_3^{\,2} \right)} \tag{2.47}$$

In this work, damage curves describing relationships between the stress triaxialities and effective plastic strains to failure were determined for onset state of microcracks and plastic instability. In sheet metal forming industry, the principal plastic strain diagram, FLD is conventionally used as an empirical failure criterion to evaluate formability of examined steel sheets. Therefore, developed damage curves for both crack initiation and plastic instability were also transformed into space of principal strain by using Equations (2.48)–(2.50).

Under the assumption of plane stress, steel sheet is basically deformed by membrane stresses, transmitted through the sheet with the through–thickness stress being negligible. There is a unique relation between the stress triaxiality η and the strain increment ratio α for an isotropic material, as shown in Equation (2.48) [52].

$$\eta = \frac{\sigma_m}{\bar{\sigma}} = \frac{1+\alpha}{\sqrt{3}\sqrt{1+\alpha+\alpha^2}} \tag{2.48}$$

In addition, the effective plastic strain for material exhibiting plastic isotropy can be defined as:

$$\mathrm{d}\bar{\varepsilon} = \frac{2\mathrm{d}\varepsilon_1}{\sqrt{3}}\sqrt{1+\alpha+\alpha^2} \tag{2.49}$$

From the relationship of strain increment in Equation (2.49), the major and minor principal plastic strain can be calculated as given in Equation (2.50).

$$\mathrm{d}\varepsilon_2 = \alpha\mathrm{d}\varepsilon_1 \tag{2.50}$$